ELSEVIER

Nuclear Physics B 555 (1999) 355–394

NUCLEAR PHYSICS B

www.elsevier.nl/locate/npe

Real-time dynamics with fermions on a lattice

Gert Aarts[a,1], Jan Smit[a,b,2]

[a] *Institute for Theoretical Physics, Utrecht University, Princetonplein 5, 3584 CC Utrecht, The Netherlands*
[b] *Institute for Theoretical Physics, University of Amsterdam, Valckenierstraat 65, 1018 XE Amsterdam, The Netherlands*

Received 18 December 1998; revised 4 May 1999; accepted 28 May 1999

Abstract

The 1 + 1-dimensional abelian Higgs model with fermions is a toy model for the theory of electroweak baryogenesis. We study the dynamics of the model with axially coupled fermions in real-time. The model is defined on a space-time lattice to preserve gauge invariance and to obtain numerical stability in a simple way. We take into account the phenomenon of lattice fermion doubling. The dynamics is approximated by treating the inhomogeneous Bose fields classically, which is justified in a large N_f approximation. The back reaction on the Bose fields due to fermion field fluctuations is calculated using a mode function expansion. We discuss and present numerical results for the response of fermions to sphaleron transitions, the renormalizability of the effective equations of motion and non-perturbative dynamics in the framework of non-equilibrium quantum field theory. The long-time behaviour of the system is discussed and we speculate about applications to finite density calculations.

PACS: 11.15.Ha; 11.15.Pg; 11.30.Fs
Keywords: Real-time dynamics; Lattice fermions; Baryogenesis

1. Introduction

The time evolution of quantum fields in and out of equilibrium plays an important role in the early universe and in heavy ion collisions. Detailed questions concerning baryogenesis, inflation, the chiral phase transition and time evolution during phase transitions in general, require a non-perturbative analysis, preferably directly in real (as opposed to

[1] E-mail: aarts@phys.uu.nl
[2] E-mail: jsmit@phys.uva.nl

0550-3213/99/$ - see frontmatter
PII S0550-3213(99)00320-X

imaginary) time. Since exact answers are usually not available, a considerable amount of work has been devoted to finding suitable approximation methods.

One approach which has received a lot of attention recently is based on Hartree or large N approximations [1–3], and has been applied to pair production in strong electric fields [4], (inflationary) cosmology [5–7], the formation of chiral condensates in heavy ion collisions [8] and non-equilibrium symmetry breaking [9]. In this approximation method, the fields are written as the sum of 'classical' or 'background' fields (which are then called order parameter, or condensate[3]) and quantum fluctuations around them. A set of coupled equations for the background fields and the fluctuations can be derived from first principles in several ways from the Schwinger–Keldysh formalism for real-time (non-)equilibrium field theory, and they have the form of semiclassical equations of motion. A nice property of the equations is that they contain only the usual quantum divergences which can be renormalized with the usual counterterms.

However, in numerical work the emphasis in the literature has been mainly on situations where the classical field is homogeneous. Although this is sufficient for some situations (inflationary scenarios, pair creation in strong homogeneous electric fields), this is certainly not the case for sphaleron transitions or realistic treatments of heavy ion collisions.

A useful toy model for obtaining a better understanding of the dynamics that plays a role in various scenarios for baryogenesis (for recent reviews, see, e.g., Ref. [10]) has been the abelian Higgs model in $1+1$ dimensions [11,12]. The model has many properties in common with the electroweak sector of the Standard Model, in particular it has a non-trivial vacuum structure which is labelled with the Chern–Simons number, and sphaleron barriers separating the vacua. Furthermore, extending it with axially coupled fermions results into a model with anomalous fermion number non-conservation, similar to baryon number violation in the Standard Model.

In this paper we study this abelian Higgs model with axial fermions, using the non-equilibrium method mentioned above. We treat the bosonic fields as classical background fields, and the fermions as fluctuations, which is justified for N_f fermions in the limit of large N_f. The bosonic fields are not restricted to be homogeneous, allowing for genuine sphaleron transitions. The equations of motion for the bosonic fields have the form of classical field equations coupled to the fermion current or force. The fermions are treated with a mode function expansion, in which the mode functions obey a Dirac-like equation in the presence of inhomogeneous background fields.

We formulate the model on a lattice in space and time. This allows for a simple and stable time integration of the coupled partial differential equations for finite lattice spacing. Furthermore, gauge invariance can be implemented and exact symmetries of the lattice action give rise to exact conservation laws at finite lattice spacing.

In the literature, to our knowledge fermion fields have been treated numerically only in the case of homogeneous mean fields [4,7] (pair production, preheating in

[3] We shall use the terms classical field, background field and order parameter interchangeably.

inflation), while fermions in the presence of inhomogeneous mean fields have so far been investigated analytically only (see e.g. Ref. [13]).

In the remainder of this Introduction, we give the outline of the paper. In Section 2, we introduce and summarize some basic properties of the abelian Higgs model with axial fermions in the continuum. In particular, we recall that the axial gauge symmetry can be transformed into a vector one, which is convenient because it allows us to extend known methods for fermions on the lattice in imaginary-time to real-time. This transformation leads to an unusual Majorana-type Yukawa coupling, hence, we go from a formulation with Dirac spinors to one with Majorana spinors. The next two sections are rather technical. In Section 3 we present the model on the lattice. Fermion fields on a lattice lead to the fermion doubling phenomenon [14–16], and we describe in this section how we deal with this. Symmetries, currents and useful observables are discussed in Section 4. The large N_f effective action is briefly derived in Section 5 and the resulting equations of motion are given in Section 6. The effective equations of motion are solved numerically and we present results in Sections 7–10. In Section 7 we use handmade time dependent Bose field configurations that go from one vacuum to another via a sphaleron transition. These external fields are used to test the properties of the fermion system. Issues related to renormalization are discussed in Section 8. In Section 9, we present numerical results for the full non-perturbative dynamics, including the fermion back reaction on the Bose fields. We discuss the long-time behaviour of the system in Section 10 and also mention a possible application to finite density. We end with a summary and outlook.

Conventions and technicalities are summarized in several appendices. Appendix A contains our conventions and in Appendix B we give the initial mode functions used for the fermions. Finally, in Appendix C we show how the relation between spectral flow and the anomalous conservation law works out in our lattice model.

2. Continuum model

We consider the abelian Higgs model in $1+1$ dimensions with axially coupled fermions. The action consists of a gauge, Higgs and fermion part and is given, in the continuum, by

$$S = S_G + S_H + S_F, \tag{2.1}$$

with

$$S_G = -\int d^2x \frac{1}{4e^2} F_{\mu\nu}F^{\mu\nu}, \tag{2.2}$$

$$S_H = -\int d^2x \left[(D_\mu\phi)^* D^\mu\phi + V(\phi)\right], \qquad V(\phi) = \lambda\left(\phi^*\phi - v^2/2\right)^2, \tag{2.3}$$

$$S_F = -\int d^2x \left[\bar{\psi}(\not{\partial} + iq\not{A}\gamma_5)\psi + G\bar{\psi}(\phi^* P_L + \phi P_R)\psi\right]. \tag{2.4}$$

Here $F_{\mu\nu} = \partial_\mu A_\nu - \partial_\nu A_\mu$, $D_\mu = \partial_\mu - iA_\mu$, and $P_{R,L} = (1 \pm \gamma_5)/2$. The model is defined on a circle with circumference L in the spatial direction. The bosonic (fermionic) fields obey (anti)periodic boundary conditions. Our conventions are summarized in Appendix A.

The model is invariant under local axial gauge transformations

$$\psi(x) \to e^{iq\xi(x)\gamma_5}\psi(x), \qquad \phi(x) \to e^{-i\xi(x)}\phi(x), \quad A_\mu(x) \to A_\mu(x) - \partial_\mu\xi(x).$$

Gauge invariance implies that the fermions have one half of the charge of the scalar field, $q = \frac{1}{2}$. The conserved (axial) current, $\partial_\mu j^\mu = 0$, associated to the global gauge symmetry, is

$$j^\mu = -j_5^\mu + j_h^\mu, \qquad j_5^\mu = iq\bar{\psi}\gamma^\mu\gamma_5\psi, \qquad j_h^\mu = i(D^\mu\phi)^*\phi - i\phi^* D^\mu\phi.$$

Furthermore there is a global vector symmetry with a classically conserved current

$$\psi \to e^{i\omega}\psi, \qquad j_f^\mu = i\bar{\psi}\gamma^\mu\psi,$$

corresponding to fermion number.

The global vector symmetry is anomalous, and the anomaly equation reads

$$\partial_\mu j_f^\mu = -q_{\text{top}}.$$

The topological charge density can be written as the divergence of the Chern–Simons current

$$q_{\text{top}} = \frac{1}{4\pi}\epsilon^{\mu\nu}F_{\mu\nu} = \partial_\mu C^\mu, \qquad C^\mu = \frac{1}{2\pi}\epsilon^{\mu\nu}A_\nu.$$

Fermion number violation is expressed as

$$Q_f(t) - Q_f(0) = -(C(t) - C(0)), \tag{2.5}$$

relating the total fermion number and the Chern–Simons number

$$Q_f(t) = \int dx^1 j_f^0(x), \qquad C(t) = \int dx^1 C^0(x) = -\frac{1}{2\pi}\int dx^1 A_1(x). \tag{2.6}$$

It is possible to transform the model to one with a vector gauge symmetry, by performing charge conjugation only on the right-handed fields [17]. This is convenient, because we want to treat the model on a lattice.[4] The transformation is explicitly

$$\psi_R = (\bar{\psi}'_R C)^T, \qquad \bar{\psi}_R = -(C^\dagger\psi'_R)^T, \qquad \psi_L = \psi'_L, \qquad \bar{\psi}_L = \bar{\psi}'_L. \tag{2.7}$$

C denotes the charge conjugation matrix. In these primed variables, the fermion part of the action is

$$S_F = -\int d^2x \left[\bar{\psi}'(\partial\!\!\!/ - iqA\!\!\!/)\psi' + \tfrac{1}{2}G\psi'^T C^\dagger\phi^*\psi' - \tfrac{1}{2}G\bar{\psi}' C\phi\bar{\psi}'^T\right]. \tag{2.8}$$

In the Yukawa mass term only the antisymmetric part survives. The gauge-fermion part of the action, with $G = 0$, has now the form of the Schwinger model, or QED in $1+1$

[4] A similar transformation can also be performed in the electroweak SU(2) Higgs model in $3+1$ dimensions.

dimensions, with $q = \frac{1}{2}$ charged fermions. The Yukawa term, coupling the fermion field to the scalar field, has turned into a Majorana-like mass term.

In terms of the primed fermion field, the gauge symmetry is vector-like

$$\psi'(x) \to e^{-iq\xi(x)}\psi'(x), \quad \phi(x) \to e^{-i\xi(x)}\phi(x), \quad A_\mu(x) \to A_\mu(x) - \partial_\mu\xi(x),$$

with the conserved current

$$j^\mu = j_f'^\mu + j_h^\mu, \qquad j_f'^\mu = iq\bar{\psi}'\gamma^\mu\psi' = -j_5^\mu.$$

The global symmetry that involves only the fermion field is now axial, with a classically conserved current

$$\psi' \to e^{-i\omega\gamma_5}\psi', \qquad j_5'^\mu = i\bar{\psi}'\gamma^\mu\gamma_5\psi' = -j_f^\mu. \tag{2.9}$$

The anomaly equation reads

$$Q_5'(t) - Q_5'(0) = C(t) - C(0), \qquad Q_5'(t) = \int dx^1 j_5'^0(x). \tag{2.10}$$

In the rest of this paper we will only work with the transformed action. Therefore we drop the primes from the fermion fields and charges in the following sections.

In the remainder of this section, we summarize some properties of the model. We work in the temporal gauge $A_0 = 0$ throughout the paper. The bosonic vacuum can be labelled with the Chern–Simons number C. The local energy minima are characterized by C being integer valued and $|\phi| = v/\sqrt{2}$. The vacua are separated by finite energy sphaleron barriers, where C is half-integer. The height of the energy barrier is given by the sphaleron energy $E_{\rm sph} = \frac{2}{3}\sqrt{2\lambda}v^3$ [18]. We will show the vacuum structure in more detail, also in the presence of fermions, when we use handmade sphaleron transitions in Section 7.

The dimensions of the fields and coupling constants is as follows: ϕ and v are dimensionless, ψ has a mass dimension of 1/2, A_μ, e and G have dimension 1, and λ has dimension 2.

Elementary powercounting shows that besides the partition function, only the one-loop self-energy of the scalar field is superficially divergent. This divergence can be cancelled with the appropriate choice for the bare scalar mass (or v^2).

Finally, the tree level masses, due to classical Higgs expectation value, of respectively the scalar, gauge and fermion fields, are

$$m_H^2 = 2\lambda v^2, \qquad m_{A,h}^2 = e^2v^2, \qquad m_F^2 = \frac{G^2v^2}{2} \quad \text{(tree level)}.$$

At the one-loop level, the fermion field not only affects the scalar self energy, it contributes also to the mass of the gauge boson

$$m_{A,f}^2 = \frac{q^2e^2}{\pi} \quad \text{(one-loop fermion)}.$$

This concludes the introduction of the model. In the next section, we discretize it on a lattice in space and time.

3. Lattice formulation

In Section 5 and beyond, we derive and study a set of effective equations of motion, that involve the Bose fields and the back reaction of the fermion field. This study is done numerically, and involves a discretization. A convenient way to discretize the equations is by use of a lattice formulation in space and real time. There are good reasons to use a lattice: exact symmetries of the lattice action give rise to exactly conserved quantities (i.e. for finite lattice spacing), the lattice distance is a gauge invariant ultraviolet cutoff, the resulting time integration algorithm is simple and stable. For a general introduction to lattice gauge theories in Euclidean space-time, we refer to Ref. [16]. Before we write down the effective equations, we first discuss in this section the lattice formulation and in the next section exact symmetries and conserved currents.

The model is defined on a lattice in space and (real) time, $x = (x^0, x^1)$. When there is no confusion we also use $x^0 = t, x^1 = x$. The lattice spacing in direction μ is denoted by $a_\mu = (a_0, a_1 \equiv a)$, and there are N spatial lattice points ($L = aN$). As indicated in the previous section, from now on we only work with the transformed action with a vector-like gauge symmetry (i.e. (2.1)–(2.3), (2.8) in the continuum), hence we drop the primes from the fermion fields and currents.

To put the Bose fields on the lattice is straightforward. We replace the (covariant) derivative by the lattice (covariant) derivative as

$$\partial_\mu f(x) = \frac{1}{a_\mu}\left[f(x+\hat{a}_\mu) - f(x)\right],$$

$$D_\mu f(x) = \frac{1}{a_\mu}\left[U_\mu(x) f(x+\hat{a}_\mu) - f(x)\right],$$

$$\partial'_\mu f(x) = \frac{1}{a_\mu}\left[f(x) - f(x-\hat{a}_\mu)\right],$$

$$D'_\mu f(x) = \frac{1}{a_\mu}\left[f(x) - U^*_\mu(x-\hat{a}_\mu) f(x-\hat{a}_\mu)\right].$$

$\hat{a}_\mu$ denotes the unit vector in the μ direction, and we use the notation

$$U_\mu(x) = e^{-ia_\mu A_\mu(x)}.$$

The gauge and scalar part of the action keep the same form as in the continuum

$$S_G = -\sum_{x,\mu,\nu} \frac{1}{4e^2} F_{\mu\nu} F^{\mu\nu}, \tag{3.1}$$

$$S_H = -\sum_{x,\mu} (D_\mu \phi)^* D^\mu \phi - \sum_x V(\phi). \tag{3.2}$$

We use the non-compact formulation for the gauge field.

To put fermions on a lattice is less straightforward. The naive way leads to so-called fermion doublers in space and time [14,15]. Instead of one physical fermion particle, the lattice action describes, close enough to the continuum limit, 2^2 physical fermions.

One effect of the doublers is to cancel the anomaly, when the naive continuum definition of Q_5 is used [15]. In the Euclidean formalism, the doublers can be removed by adding a higher derivative term to the action: the Wilson term, proportional to a parameter r [14]. Another possibility is to interpret the doublers as physical particles, i.e. the lattice action describes more than one flavour. This is the idea behind the staggered fermion method [19].

In this paper, we add a Wilson term in space, proportional to r_1, to suppress the space doublers. We interpret the doublers in time as physical particles. Hence the lattice action describes two flavours. In [20] we discuss in detail fermions on a lattice in real-time, and we construct the Hilbert space and the transfer matrix, associated to the lattice fermion path integral, which clarifies further the physical interpretation of the lattice system.

The fermion part of the lattice action is given by

$$S_F = -\sum_x \left[\bar{\psi}(\not{\bar{D}} + W)\psi + \tfrac{1}{2}G\phi^*\psi^T C^\dagger \psi - \tfrac{1}{2}G\phi\bar{\psi}C\bar{\psi}^T\right]. \tag{3.3}$$

The Dirac operator is

$$\not{\bar{D}} = \sum_\mu \gamma^\mu \bar{D}_\mu, \qquad \bar{D}_\mu = \tfrac{1}{2}\left(D_\mu + D'_\mu\right),$$

which is explicitly (we recall that the fermions have charge $q = \frac{1}{2}$)

$$\bar{D}_{\mu xy} = \frac{1}{2a_\mu}\left[\delta_{x+\hat{\mu}a_\mu,y}U^q_\mu(x) - \delta_{x,y+\hat{\mu}a_\mu}U^{q\dagger}_\mu(y)\right], \qquad U^q_\mu(x) = e^{-iqa_\mu A_\mu(x)}.$$

Note that $\bar{D}^\dagger_\mu = -\bar{D}_\mu$, and the (anti)symmetric parts are given by $\bar{D}^S_\mu = \mathrm{Im}\bar{D}_\mu, \bar{D}^A_\mu = \mathrm{Re}\bar{D}_\mu$. The Wilson term (in space and time, with parameters $r_\mu = (r_0, r_1)$), is

$$W = \sum_\mu W^\mu, \qquad W^\mu = -\tfrac{1}{2}a_\mu r_\mu D'_\mu D^\mu,$$

$$W^\mu_{xy} = -\frac{r_\mu}{2a_\mu}\left[-2\delta_{x,y} + \delta_{x+\hat{\mu}a_\mu,y}U^q_\mu(x) + \delta_{x,y+\hat{\mu}a_\mu}U^{q\dagger}_\mu(y)\right],$$

with $W^\dagger = W$, and the (anti)symmetric parts $W^S = \mathrm{Re}W, W^A = \mathrm{Im}W$. As indicated above, we use $r_0 = 0$ throughout this paper. The numerical results presented further on, are obtained using $r_1 = 1$.[5]

Because of the Majorana coupling between the scalar and the fermion field, it is convenient to use a Majorana formulation with real gamma matrices and a four-component real Majorana field Ψ. It is constructed from the real and imaginary parts of ψ,

[5] In the original model of the previous section, the Wilson term corresponds to a Majorana–Wilson term

$$S_{FW} = -\sum_x \left[\psi^T C^\dagger P_L W\psi - \bar{\psi}P_R C W\bar{\psi}^T\right].$$

$$\psi = \frac{1}{\sqrt{2}}(\Psi_1 - i\Psi_2), \qquad \psi^\dagger = \frac{1}{\sqrt{2}}(\Psi_1^T + i\Psi_2^T), \qquad \Psi = \begin{pmatrix} \Psi_1 \\ \Psi_2 \end{pmatrix}.$$

We also introduce Pauli matrices, written as $\rho_{1,2,3}$, that act on the 1,2 components of Ψ.

In terms of Ψ and the ρ_i matrices, the fermion part of the action can be written as

$$\begin{aligned} S_F &= -\sum_x \tfrac{1}{2}\Psi^T\beta\left[\not{D}^A + \rho_2\not{D}^S + W^S + \rho_2 W^A + \frac{G}{\sqrt{2}}(\phi_1\rho_3 + \phi_2\rho_1)\right]\Psi \\ &\equiv -\sum_x \tfrac{1}{2}\Psi^T\beta\left[\not{\mathcal{D}} + \mathcal{W} + G\Phi\right]\Psi. \end{aligned}$$

Here we defined the covariant derivative and the Wilson term on a Majorana field as

$$\mathcal{D}_\mu = \bar{D}_\mu|_{q\to q\rho_2}, \qquad \mathcal{W} = W|_{q\to q\rho_2},$$

i.e.

$$U_\mu^q(x) \to \mathcal{U}_\mu^q(x) = e^{-iq\rho_2 a_\mu A_\mu(x)};$$

$q\rho_2$ is the Majorana charge matrix. For the Yukawa part we used the explicit representation $C = \beta$,

$$\phi = \frac{1}{\sqrt{2}}(\phi_1 - i\phi_2),$$

and we introduced a matrix field notation

$$\Phi = \frac{1}{\sqrt{2}}(\phi_1\rho_3 + \phi_2\rho_1).$$

The lattice field equation (in the temporal gauge) reads

$$\tfrac{1}{2}i(\partial_0 + \partial_0')\Psi = \mathcal{H}_D\Psi, \tag{3.4}$$

where the Majorana Dirac Hamiltonian is given by ($\alpha^1 = -\gamma^0\gamma^1$)

$$\mathcal{H}_D = -i\alpha^1\mathcal{D}_1 + \beta(\mathcal{W}^1 + G\Phi). \tag{3.5}$$

It is hermitian and antisymmetric (${\mathcal{H}_D}^\dagger = \mathcal{H}_D = -{\mathcal{H}_D}^T$).

The lattice fermion doublers in space are removed by the Wilson term in space. We now describe how we deal with fermion doubling due to the 'naive' time discretization ($r_0 = 0$). Reverting to ordinary Dirac notation, the free fermion lattice propagator is given by

$$S(p,\omega) = \frac{m_{Fp} - i\gamma_1 a^{-1}\sin ap + i\gamma^0 a_0^{-1}\sin a_0\omega}{m_{Fp}^2 + a^{-2}\sin^2 ap - a_0^{-2}\sin^2 a_0\omega}. \tag{3.6}$$

The fermion mass term $m_{Fp} = m_F + m_p$ is the sum of the physical continuum mass term m_F and a term due to the higher derivative in space, the Wilson 'mass term', $m_p = a^{-1}r_1(1-\cos ap)$. This propagator takes the usual continuum form for $a, a_0 \to 0$. However, the propagator has also a pole near $a_0\omega = \pm\pi$, corresponding to the rapid time

variation $(-1)^{t/a_0}$. As shown in [15], such poles have to be interpreted as particles, the doublers. Their physical frequency p^0 is related to ω by $a_0\omega = \pi + a_0 p^0$, such that we recover the continuum propagator in the limit $a, a_0 \to 0$, up to the unitary transformation $i\beta\gamma_5 = -\gamma_1$,

$$S\left(p, \frac{\pi}{a_0} + p^0\right) \to \gamma_1 \left(\frac{m_F - i\gamma_1 p + i\gamma^0 p^0}{m_F^2 + p^2 - p_0^2}\right) \gamma_1. \tag{3.7}$$

Hence, the lattice fermion field ψ describes *two* physical fields in the continuum limit, which we label with flavour indices u, d, and denote with χ_u and χ_d,

$$\psi(x,t) \to \chi_u(x,t) - (-1)^{t/a_0}\gamma_1 \chi_d(x,t). \tag{3.8}$$

In Majorana notation, $\chi = (X_1 - iX_2)/\sqrt{2}$, this takes the form

$$\Psi(x,t) \to X_u(x,t) - (-1)^{t/a_0}\gamma_1\rho_2 X_d(x,t). \tag{3.9}$$

Substitution in the lattice action displays its physical content in the continuum limit

$$S_F \to -\int d^2x\, \tfrac{1}{2} X^T \beta \left[\gamma^\mu D_\mu + G\Phi\tau_3\right] X. \tag{3.10}$$

Here we combined $X_{u,d}$ into a flavour doublet X on which Pauli matrices $\tau_{1,2,3}$ act. Cross terms $\propto (-1)^{t/a_0}$ do not contribute in the continuum limit. A useful relation is

$$\gamma_1\rho_2 \mathcal{H}_D(+G)\gamma_1\rho_2 = -\mathcal{H}_D(-G). \tag{3.11}$$

The Majorana Yukawa coupling happens to break the SU(2) flavour symmetry of the continuum limit of the $G = 0$ theory. Experience with Euclidean lattice fermions suggests that it could be avoided, if so desired, and that we can obtain a wide class of target continuum theories in a more sophisticated staggered fermion formulation.

It is convenient to formulate the back reaction of the fermions on the Bose fields (in Sections 5 and beyond) in terms of initial expectation values of fermion operators. This calls for an extension of (3.9) to an operator equation. Since the continuum fields X_u, X_d are supposed to be slowly varying in lattice units, they are somewhat spread out over the lattice. A minimal spreading in time is over two time slices, which is also used in derivations of the quantum mechanical Hilbert space from the lattice path integral [21]. Labelling pairs of time slices by an integer k, we may write without 'overcounting', for even $t/a_0 = 2k$,

$$\begin{aligned} \Psi(x,t) &= X_u(x,t) - \gamma_1\rho_2 X_d(x,t), \\ \Psi(x,t+a_0) &= X_u(x,t) + \gamma_1\rho_2 X_d(x,t), \end{aligned} \tag{3.12}$$

This relation suggests that it is also useful to combine $\Psi(x,t)$ and $\Psi(x,t+a_0)$ in a doublet,

$$\Xi(x,k) = \frac{1}{\sqrt{2}} \begin{pmatrix} \Psi(x,t+a_0) \\ \Psi(x,t) \end{pmatrix}, \tag{3.13}$$

so that (3.12) can be written concisely as

$$\Xi = RX, \tag{3.14}$$

with

$$R = \frac{1}{\sqrt{2}} \begin{pmatrix} 1 & \gamma_1\rho_2 \\ 1 & -\gamma_1\rho_2 \end{pmatrix}, \qquad RR^\dagger = 1, \qquad RR^T = \tau_1. \tag{3.15}$$

Eqs. (3.12) (or equivalently (3.14)) can now be viewed as relations between operators. In [20] we will give more details on the Hilbert space aspects of fermion doubling in real time. For now we assume that the physical Majorana fields X correspond to hermitian operators satisfying the anticommutation relations

$$\{X(x,t), X^T(y,t)\} = \delta_{x,y}. \tag{3.16}$$

Note that as operators, the Ψ's are not hermitian because of the imaginary ρ_2. Typically, it is the Grassmann variables $\psi(x, t+a_0)$ and $\psi^+(x,t)$ which correspond to hermitian conjugate operators in Hilbert space [21,20].

We can expand the fields X in eigenspinors of the Dirac Hamiltonian in flavour space,

$$\mathcal{H}_{Dfl} = -i\alpha^1\mathcal{D}_1 + \beta(\mathcal{W}^1 + \tau_3 G\Phi), \tag{3.17}$$

and identify the coefficients in the expansion with creation and annihilation operators. For example, let $\tilde{U}_{\alpha u}(x), \tilde{U}_{\alpha d}(x)$ be a complete orthonormal set of positive energy[6] eigenspinors of $\mathcal{H}_{Dfl}$ at $t = 0$. Here α labels the set (which typically contains momentum), and u, d indicates the flavour. We then expand

$$X_u(x,0) = \sum_\alpha \left[b_{\alpha u}\tilde{U}_{\alpha u}(x) + b^\dagger_{\alpha u}\tilde{U}^*_{\alpha u}(x) \right], \tag{3.18}$$

and similar for d. The creation and annihilation operators obey the usual anticommutation relations

$$\{b^\dagger_{\alpha f}, b_{\alpha' f'}\} = \delta_{\alpha\alpha'}\delta_{ff'}, \quad f = u, d. \tag{3.19}$$

We can now express the lattice field Ψ at time slices $t/a_0 = 0, 1$ in terms of the eigenspinors and the operators, if we combine (3.18) with (3.12) at $k = 0$. This gives

$$\Psi(x,0) = \sum_\alpha \left[b_{\alpha u}\tilde{U}_{\alpha u}(x) + b^\dagger_{\alpha u}\tilde{U}^*_{\alpha u}(x) - b_{\alpha d}\gamma^1\rho_2\tilde{U}_{\alpha d}(x) - b^\dagger_{\alpha d}\gamma^1\rho_2\tilde{U}^*_{\alpha d}(x) \right],$$

$$\Psi(x,a_0) = \sum_\alpha \left[b_{\alpha u}\tilde{U}_{\alpha u}(x) + b^\dagger_{\alpha u}\tilde{U}^*_{\alpha u}(x) + b_{\alpha d}\gamma^1\rho_2\tilde{U}_{\alpha d}(x) + b^\dagger_{\alpha d}\gamma^1\rho_2\tilde{U}^*_{\alpha d}(x) \right].$$

This relation can be extended to arbitrary times by writing

[6] The negative energy solutions are given by $\tilde{U}^*$.

$$\Psi(x,t) = \sum_{\alpha} \left[b_{\alpha u} U_{\alpha u}(x,t) + b^{\dagger}_{\alpha u} U^{*}_{\alpha u}(x,t) - b_{\alpha d} U_{\alpha d}(x,t) + b^{\dagger}_{\alpha d} U^{*}_{\alpha d}(x,t) \right], \tag{3.20}$$

where $U_{\alpha u}(x,t), U_{\alpha d}(x,t)$ are solutions of the lattice Dirac equation (3.4), with the initial conditions

$$\begin{aligned} U_{\alpha u}(x,0) &= U_{\alpha u}(x,a_0) = \tilde{U}_{\alpha u}(x), \\ U_{\alpha d}(x,0) &= -U_{\alpha d}(x,a_0) = \gamma^1 \rho_2 \tilde{U}_{\alpha d}(x). \end{aligned} \tag{3.21}$$

We shall refer to the $U(x,t)$'s as the mode functions. We show in [20] that solving the Dirac equation for the mode functions U is equivalent to time evolution in Hilbert space by means of the transfer operator. Note that (3.21) shows that the ordinary modes start smoothly in time, while the doubler modes start like $(-1)^{t/a_0}$.

The mode functions remain orthonormal under the discrete time evolution in the appropriate inner product. In terms of

$$V_{\alpha f}(k) = \frac{1}{\sqrt{2}} \begin{pmatrix} U_{\alpha f}(t+a_0) \\ U_{\alpha f}(t) \end{pmatrix}, \qquad t = 2ka_0, \qquad f = u,d, \tag{3.22}$$

where we suppress the space dependence, the time evolution can be written as

$$\begin{aligned} V_{\alpha f}(k+1) &= M(k)\, V_{\alpha f}(k), \\ M(k) &= \begin{pmatrix} 1 - 4a_0^2 \mathcal{H}_{D2k+2} \mathcal{H}_{D2k+1} & -i2a_0 \mathcal{H}_{D2k+2} \\ -i2a_0 \mathcal{H}_{D2k+1} & 1 \end{pmatrix}, \end{aligned}$$

where the subscript k indicates the time dependence of the Bose fields in the Majorana Dirac Hamiltonian. The matrix M is unitary in 'the τ_1 inner product', $M^{\dagger}\tau_1 M = \tau_1$ and it follows that the norm of the $V's$ is conserved in this inner product. The orthonormality relations follow from the initial conditions: $V^{\dagger}_{\alpha f}(0)\tau_1 V_{\alpha' f'}(0) = \delta_{\alpha\alpha'}(\tau_3)_{ff'}$. Similarly the anticommutation relations of the lattice Majorana field are preserved: $\{\Xi(x,k), \Xi^T(y,k)\} = \tau_1 \delta_{x,y}$, which follows directly from (3.14)–(3.16). These conservation relations have the same meaning as the Wronskian condition [5–9]. They imply that the basic anticommutation relations, (3.16) and (3.19), remain valid also for times larger than zero.

To summarize this section, we have formulated the model of Section 2 on a space-time lattice. A large part has been devoted to the physical interpretation of the lattice fermion field. It represents two physical fermion fields in the continuum. In relation with the dynamics to be treated in Sections 5 and beyond, the important result of this section is the mode function expansion of the lattice field (3.20) in terms of time independent operators (3.19) and spinor mode functions. These mode functions are solutions of the Dirac equation (3.4) with initial conditions (3.21).

4. Symmetries, currents and observables

We discuss several exact symmetries of the lattice action, since these lead to exactly conserved currents for finite lattice spacing. Furthermore, we construct other observables that are related to symmetries of the continuum theory.

The local gauge symmetry under which the action is invariant, acts on the fields as

$$\begin{aligned} A_\mu(x) &\to A_\mu(x) - \partial_\mu \xi(x), & U_\mu(x) &\to e^{-i\xi(x)} U_\mu(x) e^{i\xi(x+\hat{a}_\mu)}, \\ \phi(x) &\to e^{-i\xi(x)}\phi(x), & \Phi(x) &\to e^{-iq\rho_2\xi(x)}\Phi(x)e^{iq\rho_2\xi(x)}, \\ \psi(x) &\to e^{-iq\xi(x)}\psi(x), & \Psi(x) &\to e^{-iq\rho_2\xi(x)}\Psi(x). \end{aligned}$$

We indicated how the fields transform for the different ways in which they are written.

The global gauge symmetry leads to the conserved current $j^\mu(x) = j_h^\mu(x) + j_f^\mu(x)$, with the scalar part

$$j_h^\mu(x) = i(D^\mu\phi(x))^*\phi(x) - i\phi^*(x)D^\mu\phi(x), \tag{4.1}$$

and the fermion part (in Dirac and in Majorana notation)

$$\begin{aligned} j_f^\mu(x) &= iq\left[\bar{\psi}(x+\hat{a}_\mu)P_+^\mu U_\mu^{q\dagger}(x)\psi(x) - \bar{\psi}(x)P_-^\mu U_\mu^q(x)\psi(x+\hat{a}_\mu)\right] \\ &= \frac{i}{2}\left[\Psi^T(x+\hat{a}_\mu)\beta P_+^\mu q\rho_2 \mathcal{U}_\mu^{q\dagger}(x)\Psi(x) - \Psi^T(x)\beta P_-^\mu q\rho_2\mathcal{U}_\mu^q(x)\Psi(x+\hat{a}_\mu)\right]. \end{aligned} \tag{4.2}$$

We use the notation, familiar from Euclidean lattice fermions, $P_\pm^\mu = (r_\mu \pm \gamma^\mu)/2$ (recall that $r_0 = 0$). It is easy to check what this current represents in terms of the flavour fields X_u, X_d, using the relations (3.12). For example, the charge density at even t/a_0 is

$$\begin{aligned} j_f^0(x,t) &= \tfrac{1}{4}\left[\Psi^T(x,t+a_0)q\rho_2\Psi(x,t) + \Psi^T(x,t)q\rho_2\Psi(x,t+a_0)\right] \\ &= \tfrac{1}{2}\left[X_u^T(x,t)q\rho_2 X_u(x,t) + X_d^T(x,t)q\rho_2 X_d(x,t)\right], \end{aligned}$$

which is precisely the charge density due to two Majorana fermions with charge q, as expected.

There is another global symmetry, due to the fact that the model is defined on a lattice. It is inspired by the staggered fermion formalism. It is

$$\Psi(x,t) \to \exp\left[i\omega\gamma^1(-1)^{t/a_0}\right]\Psi(x,t).$$

The associated charge density is

$$j_{\not h}^0(x,t) = \frac{(-1)^{t/a_0}}{4}\left[\Psi^T(x,t)\gamma^1\Psi(x,t+a_0) - \Psi^T(x,t+a_0)\gamma^1\Psi(x,t)\right].$$

The physical interpretation becomes clear in terms of the flavour fields. At even t/a_0,

$$\begin{aligned} j_{\not h}^0(x,t) &= \tfrac{1}{2}\left[X_u^T(x,t)\rho_2 X_d(x,t) + X_d^T(x,t)\rho_2 X_u(x,t)\right] \\ &= \tfrac{1}{2}X^T(x,t)\rho_2\tau_1 X(x,t), \end{aligned}$$

where the last line is written compactly in flavour space. It is the first component of the flavour triplet current.

Other observables, which are not directly related to a symmetry of the lattice action, are constructed with the continuum limit as a guidance. The energy density of the fermions is found to be

$$H_f(x,t) = \tfrac{1}{4}\left[\Psi^T(x,t)\mathcal{H}_D(x,t)\Psi(x,t) + (t \to t+a_0)\right]. \tag{4.3}$$

In terms of the flavour fields at even t/a_0, using again (3.12), this is the expected energy density

$$H_f(x,t) = \tfrac{1}{2}X^T(x,t)\mathcal{H}_{D\mathrm{fl}}(x,t)X(x,t),$$

where $\mathcal{H}_{D\mathrm{fl}}$ was defined in (3.17), and we used (3.11). The anomalous axial vector current which satisfies the anomaly equation is the flavour singlet current, i.e. where the contributions from both flavours add,

$$\begin{aligned} j_5^0(x,t) &= \tfrac{1}{2}X^T(x,t)\gamma_5\rho_2 X(x,t) \\ &= \tfrac{1}{2}\left[X_u^T(x,t)\gamma_5\rho_2 X_u(x,t) + X_d^T(x,t)\gamma_5\rho_2 X_d(x,t)\right]. \end{aligned}$$

It is straightforward to verify for even t/a_0, that in terms of the lattice field the axial charge density is obtained by taking

$$j_5^0(x,t) = \tfrac{1}{4}\left[\Psi^T(x,t)\gamma_5\rho_2\Psi(x,t) + (t \to t+a_0)\right].$$

We will divide, in the rest of the paper, the axial charge (density) by a factor of two to keep the anomaly equation, given in Section 2: $Q_5(t) - Q_5(0) = C(t) - C(0)$.

The current associated with the global symmetry $\psi \to \exp(-i\omega\gamma_5)\psi$ of the continuum action, is given by

$$\begin{aligned} j_{\mathrm{fl}5}^{\mu}(x) &= \frac{i}{2}\left[\bar{\psi}(x)\gamma^{\mu}\gamma_5 U_{\mu}^{q}(x)\psi(x+\hat{a}_{\mu}) + \bar{\psi}(x+\hat{a}_{\mu})\gamma^{\mu}\gamma_5 U_{\mu}^{q\dagger}(x)\psi(x)\right], \\ &= \frac{i}{4}\left[\Psi^T(x)\beta\gamma^{\mu}\gamma_5\rho_2\mathcal{U}_{\mu}^{q}(x)\Psi(x+\hat{a}_{\mu}) + \Psi^T(x+\hat{a}_{\mu})\beta\gamma^{\mu}\gamma_5\mathcal{U}_{\mu}^{q\dagger}(x)\Psi(x)\right]. \end{aligned}$$

The continuum interpretation of this current is not that it represents the anomalous axial vector current, but rather the third component of the flavour *triplet* axial vector current. For example, the charge density at even t/a_0 is

$$\begin{aligned} j_{\mathrm{fl}5}^{0}(x,t) &= \tfrac{1}{4}\left[\Psi^T(x,t+a_0)\gamma_5\rho_2\Psi(x,t) + \Psi^T(x,t)\gamma_5\rho_2\Psi(x,t+a_0)\right] \\ &= \tfrac{1}{2}\left[X_u^T(x,t)\gamma_5\rho_2 X_u(x,t) - X_d^T(x,t)\gamma_5\rho_2 X_d(x,t)\right] \\ &= \tfrac{1}{2}X^T(x,t)\gamma_5\rho_2\tau_3 X(x,t). \end{aligned}$$

Indeed, this density represent the difference between the two axial charge densities instead of the sum. This is known in the naive fermion formalism as well [15]. The current is not exactly conserved because the global symmetry is broken explicitly on the lattice by the Wilson term in space.

After this lengthy discussion of the model and its lattice version, we come to the effective action and equations of motion in the following section.

5. Large N_f effective action

In this section we derive the effective action by solving the path integral to leading order in the large N_f approximation. Since this can already be found in great detail in the literature [2,3], we only show the essential steps. The effective equations of motion follow directly from the effective action.

To avoid a notational jam, it is convenient to denote the Bose fields collectively with $\varphi = (\phi, \phi^*, A_\mu)$. We also denote the corresponding sources as $J = (J^*, J, J^\mu)$. We use a compact notation, such that e.g. $J \cdot \varphi = \sum J(x)\varphi(x)$, where the sum is over all indices, including space-time.

The partition function we are interested in is

$$Z[J] = \mathrm{Tr}\,\rho T_C \exp iJ \cdot \varphi. \tag{5.1}$$

T_C indicates that the exponent is time ordered along the Keldysh contour in the complex time plane, which is shown in Fig. 1. We take the initial density matrix ρ such that the fermion field has zero mean value. Matrix elements of the initial density matrix are written as

$$\langle \varphi_a, \Psi_a | \rho | \varphi_b, \Psi_b \rangle = \rho(\varphi_a, \Psi_a; \varphi_b, \Psi_b).$$

The corresponding path integral expression reads

$$Z[J] = \int \mathcal{D}\varphi_a \mathcal{D}\varphi_b \mathcal{D}\Psi_a \mathcal{D}\Psi_b\, \rho(\varphi_a, \Psi_a; \varphi_b, \Psi_b) \int_C \mathcal{D}\varphi \mathcal{D}\Psi \exp(iS + iJ \cdot \varphi), \tag{5.2}$$

with $S = S_B + S_F$, $S_B = S_G + S_H$. The c again denotes that the whole expression is defined along the Keldysh contour. The initial values of the fields and correlations are determined by the density matrix.

Let us for a moment consider the part of the partition function that involves the fermion field. Formally, we can perform the integration over the fermion field, and we denote the result as

$$\tfrac{1}{2} \log D[\varphi] \equiv \log \int \mathcal{D}\Psi_a \mathcal{D}\Psi_b\, \rho(\varphi_a, \Psi_a; \varphi_b, \Psi_b) \int_C \mathcal{D}\Psi \exp iS_F[\varphi]. \tag{5.3}$$

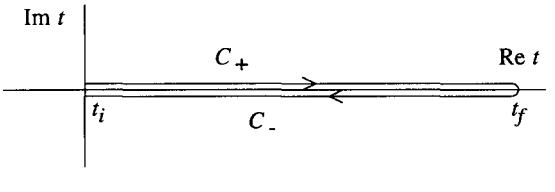

Fig. 1. Keldysh contour in the complex time plane.

$D[\varphi]$ depends on the Bose fields φ along the contour, including the initial Bose fields φ_a, φ_b. Note that if the density matrix is quadratic in Ψ, D represents the resulting determinant. We would like to remark that it is not necessary to have a gaussian density matrix for Ψ to perform the integration. Furthermore, we do not need to specify any property of the density matrix regarding its Bose field dependence.

To arrive at a large N_f expansion, we duplicate the field Ψ N_f times, and demand that all fields Ψ^i are initialized with the same density matrix, i.e.

$$\Psi \to \Psi^i, \qquad \rho(\varphi_a, \Psi_a; \varphi_b, \Psi_b) \to \prod_i \rho(\varphi_a, \Psi_a^i; \varphi_b, \Psi_b^i), \qquad i = 1, \ldots, N_f.$$

If we then integrate out the fermion fields, we find

$$Z[J] = \int \mathcal{D}\varphi_a \mathcal{D}\varphi_b \int_C \mathcal{D}\varphi \exp i \left(S_B - i\tfrac{1}{2} N_f \log D + J \cdot \varphi \right).$$

To proceed, it is common use to rescale the parameters, and the Bose fields and sources such that the exponent in the path integral becomes proportional to N_f. In our model, this rescaling is explicitly

$$\phi = \phi' \sqrt{N_f}, \quad v = v' \sqrt{N_f}, \quad J = J' \sqrt{N_f},$$
$$e = e' / \sqrt{N_f}, G = G' / \sqrt{N_f}, \lambda = \lambda' / N_f.$$

Note that this rescaling implies that the original, unscaled theory is weakly coupled when N_f is large, and that the initial conditions for the unscaled ϕ and A_μ / e have to be such that they are of order $\sqrt{N_f}$.

In terms of the primed variables, the partition function is (up to normalization)

$$Z[J'] = \int \mathcal{D}\varphi_a' \mathcal{D}\varphi_b' \int_C \mathcal{D}\varphi' \exp i N_f \left(S_B' - i\tfrac{1}{2} \log D' + J' \cdot \varphi' \right). \tag{5.4}$$

which suggests a saddle point expansion for large N_f. The field configurations that determine the stationary phase, φ_s, are found by extremizing the exponent of (5.4).

A Legendre transformation from the generating functional $\log Z$ depending on the sources, to the effective action depending on the so-called classical or mean fields,

$$Z[J'] = \exp i N_f W[J'], \qquad \bar{\varphi} = \frac{\partial W[J']}{\partial J'}, \qquad \Gamma[\bar{\varphi}] = W[J'] - J' \cdot \bar{\varphi},$$

yields the effective action, which is to leading order in large N_f,

$$\Gamma[\bar{\varphi}] = S_B[\bar{\varphi}] - \frac{i}{2} \log D[\bar{\varphi}].$$

The effective equations of motion follow from

$$\frac{\partial \Gamma[\bar{\varphi}]}{\partial \bar{\varphi}} = -J'.$$

The mean fields $\bar{\varphi}$ are defined on the complete Keldysh contour. In general, the sources J are different on the upper and lower part of the contour (which is needed

to be able to construct correlation functions of arbitrary observables). This implies that also the mean fields are different. However, having derived the equations of motion and expressions for the observables, we can set the upper and lower sources equal, which implies that the upper and lower mean fields are also the same. The initial conditions are in principle to be derived from the density matrix. This can be analyzed conveniently if it has a gaussian form. To leading order $\varphi_s = \bar{\varphi}$ [2].

Differentiating $\log D$ at $t > t_i$ gives the back reaction of the fermion field in the background of the Bose fields, at time t. We use a bracket notation to denote the result

$$\tfrac{1}{2}\frac{\partial}{\partial\bar{\varphi}(x,t)}\log D \equiv i\left\langle\frac{\partial S_F}{\partial\varphi(x,t)}\right\rangle.$$

The initial conditions for the fermion field are also determined by (5.3). However, we find that is more transparent to use the operator formalism. We discuss the fermion initial conditions in the following section.

To conclude this section, we would like to remark that in this approximation scheme the fermion fields are integrated out exactly. The large N_f approximation is only used to justify a saddle point expansion of the resulting effective bosonic action. The leading order result in this expansion is that the Bose fields are treated classically, and the fermions show up in a one-loop contribution, but with the exact propagator. In the following, we drop the bars from the mean fields.

6. Effective equations of motion

We are now in a position to give the effective equations of motion. Using the results from the previous section, we find the bosonic field equations (in the temporal gauge)

$$\partial_0'\partial_0 A_1(x,t) = e^2\left[j_h^1(x,t) + \left\langle j_f^1(x,t)\right\rangle\right], \tag{6.1}$$

$$\partial_1'\partial_0 A_1(x,t) = -e^2\left[j_h^0(x,t) + \left\langle j_f^0(x,t)\right\rangle\right], \tag{6.2}$$

$$\partial_0'\partial_0\phi(x,t) = D_1'D_1\phi(x,t) - 2\lambda\left[|\phi(x,t)|^2 - v_B^2/2\right]\phi(x,t) + G\left\langle F(x,t)\right\rangle. \tag{6.3}$$

The scalar and fermion contribution to the current, j_h^μ and j_f^μ respectively, are given by (4.1) and (4.2). The force on the Higgs field due to the fermions is defined by

$$F(x,t) \equiv \frac{1}{G}\frac{\partial S_F}{\partial\phi^*(x,t)} = i\tfrac{1}{4}\Psi^T(x,t)\beta(\rho_1 + i\rho_3)\Psi(x,t). \tag{6.4}$$

Eq. (6.2) is Gauss' law. It implies (on a periodic lattice) that the total charge is zero,

$$Q(t) = Q_h(t) + Q_f(t) = \sum_x\left(j_h^0(x,t) + \left\langle j_f^0(x,t)\right\rangle\right) = 0. \tag{6.5}$$

In (6.3), we used a subscript B to indicate that v_B^2 is a bare parameter. We will discuss renormalization in Section 8.

Following Refs. [4–9] for the case of homogeneous classical fields, we calculate the back reaction of the fermions on the Bose fields using a mode function expansion, introduced in Section 3. We expand the field Ψ in a complete set of eigenspinors of the initial Dirac Hamiltonian, with time-independent creation and annihilation operators as coefficients (i.e. (3.20))

$$\Psi(x,t) = \sum_{\alpha} \left[b_{\alpha u} U_{\alpha u}(x,t) + b^{\dagger}_{\alpha u} U^{*}_{\alpha u}(x,t) - b_{\alpha d} U_{\alpha d}(x,t) + b^{\dagger}_{\alpha d} U^{*}_{\alpha d}(x,t) \right]. \tag{6.6}$$

Expectation values of the operators determine the initial quantum state of the fermion field. Two typical choices are a vacuum and a thermal state. These are given by the following expectation values

$$\left\langle b^{\dagger}_{\alpha f} b_{\alpha' f'} \right\rangle = n_{\alpha f} \delta_{\alpha\alpha'} \delta_{ff'} \qquad \left\langle b_{\alpha f} b^{\dagger}_{\alpha' f'} \right\rangle = (1 - n_{\alpha f}) \delta_{\alpha\alpha'} \delta_{ff'}, \qquad f = u, d.$$

Here $n_{\alpha f}$ is the Fermi–Dirac distribution

$$n_{\alpha f} = [\exp(E_{\alpha f}/T_{f,\mathrm{in}}) + 1]^{-1}, \tag{6.7}$$

with $E_{\alpha f}$ the eigenvalue of the Dirac Hamiltonian for eigenspinor $U_{\alpha f}$, and $T_{f,\mathrm{in}}$ the initial temperature of the fermions. We will often encounter

$$\left\langle [b_{\alpha f}, b^{\dagger}_{\alpha f}] \right\rangle = 1 - 2n_{\alpha f} \equiv \sigma_{\alpha f}. \tag{6.8}$$

All fermion observables can now be expressed in terms of $\sigma_{\alpha f}$ and the mode functions. Regarding the numerical results that are presented in this paper, we restrict ourselves to initial fermions in vacuum, i.e. $T_{f,\mathrm{in}} = 0$, for which $n_{\alpha f}$ vanishes of course.

The system is closed by giving the equation of motion for these mode functions. As explained in detail in Section 3, both $U_{\alpha u}$ and $U_{\alpha d}$ are solutions of the lattice Dirac equation (3.4),

$$\tfrac{1}{2} i(\partial_0 + \partial'_0) U_{\alpha f}(x,t) = \mathcal{H}_D \left[A_1(x,t), \phi(x,t) \right] U_{\alpha f}(x,t), \qquad f = u, d, \tag{6.9}$$

with initial conditions (3.21). The number of partial differential equations that has to be solved is quite large. Besides the Bose fields, there are $4N$ four-component complex mode functions, which make the numerical calculation scale as N^3 (for fixed a_0/a).

To be explicit, we list the fermion field expectation values in terms of the mode functions. To avoid too lengthy formulas, we combine the two flavour mode functions in one,

$$U_{\alpha} = \begin{pmatrix} U_{\alpha u} \\ U_{\alpha d} \end{pmatrix},$$

and use for the expectation values (6.8) the matrix

$$\sigma_{\alpha} = \begin{pmatrix} \sigma_{\alpha u} & 0 \\ 0 & -\sigma_{\alpha d} \end{pmatrix}.$$

We stress however that the mode functions are still to be solved with the original Dirac Hamiltonian (i.e. not the one in flavour space).

In the equations of motion we need the charge and current density, and the force the fermions exert on the scalar field. These are given by

$$\langle j_f^0(x,t)\rangle = -\tfrac{1}{4}\sum_\alpha \left[U_\alpha^\dagger(x,t)q\rho_2\sigma_\alpha U_\alpha(x,t+a_0) + U_\alpha^\dagger(x,t+a_0)q\rho_2\sigma_\alpha U_\alpha(x,t)\right],$$

$$\langle j_f^1(x,t)\rangle = \frac{i}{2}\sum_\alpha \left[U_\alpha^\dagger(x,t)\beta P_-^1 q\rho_2\sigma_\alpha \mathcal{U}_1^q(x,t)U_\alpha(x+a,t)\right.$$
$$\left. -U_\alpha^\dagger(x+a,t)\beta P_+^1 q\rho_2\sigma_\alpha \mathcal{U}_1^{q\dagger}(x,t)U_\alpha(x,t)\right],$$

$$\langle F(x,t)\rangle = -\frac{i}{4}\sum_\alpha \left[U_\alpha^\dagger(x,t)\beta(\rho_1+i\rho_3)\sigma_\alpha U_\alpha(x,t)\right].$$

Two observables we are interested in are the anomalous axial charge and the conserved flavour charge. Their densities are

$$\langle j_5^0(x,t)\rangle = -\tfrac{1}{4}\sum_\alpha \left[U_\alpha^\dagger(x,t)\gamma_5\rho_2\sigma_\alpha U_\alpha(x,t) + (t\to t+a_0)\right],$$

$$\langle j_{\rm fl}^0(x,t)\rangle = \frac{(-1)^{t/a_0}}{4}\sum_\alpha \left[U_\alpha^\dagger(x,t+a_0)\gamma_1\sigma_\alpha U_\alpha(x,t) - U_\alpha^\dagger(x,t)\gamma_1\sigma_\alpha U_\alpha(x,t+a_0)\right].$$

Finally, the energy density of the fermions is

$$E_f(x,t) = -\tfrac{1}{4}\sum_\alpha \left[U_\alpha^\dagger(x,t)\mathcal{H}_D(x,t)\sigma_\alpha U_\alpha(x,t) + (t\to t+a_0)\right].$$

All these formulas are valid for a complete set of mode functions that are initially eigenspinors of an arbitrary Dirac Hamiltonian, i.e. a Dirac Hamiltonian with arbitrary Bose fields as background. In the numerical treatment of the equations we present in the following sections, we use as initial background fields for the Dirac Hamiltonian a vacuum configuration of Bose fields, i.e. $A_1 = 0, \phi = v_R/\sqrt{2}$, where v_R is the renormalized vacuum expectation value. In terms of the density matrix, this means that we take no initial correlations between the Bose and the fermion fields, $\rho = \rho_B \otimes \rho_F$, and that ρ_F is quadratic in Ψ. In Appendix B we calculate the eigenvalues and eigenspinors in such a configuration, with the following results.

The energy eigenvalues can be summarized as

$$E_{p\eta} = \sqrt{s_p^2 + m_{p\eta}^2},$$

with

$$s_p = a^{-1}\sin pa, \qquad m_{p\eta} = m_p + \eta m_F, \qquad \eta = \pm.$$

Here p is discrete and takes N values, given by (B.2). The total fermion mass is sum or difference between the mass due to the Wilson term, $m_p = a^{-1}r_1(1-\cos pa)$, and the mass due to the Higgs vacuum expectation value, $m_F = Gv_R/\sqrt{2}$. The collective label is

now explicit, $\alpha = (p, \eta)$, and has $2N$ values. For these initial conditions, we find that the charge and current densities vanish initially,

$$\langle j_f^0(x,0)\rangle = \langle j_f^1(x,0)\rangle = \langle j_5^0(x,0)\rangle = \langle j_{\rm fl}^0(x,0)\rangle = 0.$$

The initial fermion force on the scalar field is

$$\langle F(x,0)\rangle = \langle F(x,a_0)\rangle = \frac{1}{2L}\sum_{p\eta}\sigma_{p\eta}\frac{\eta m_{p\eta}}{E_{p\eta}}. \tag{6.10}$$

The initial energy density

$$E_f(x,0) = -\frac{1}{L}\sum_{p\eta}\sigma_{p\eta}E_{p\eta}$$

contains the zero temperature divergent part ($\sigma_{p\eta} \to 1$). We renormalize this by subtracting the bare fermion energy density,

$$E_f^R(x,t) = E_f(x,t) - E_f^B, \qquad E_f^B = -\frac{1}{L}\sum_{p\eta}E_{p\eta}. \tag{6.11}$$

The total energy of the system $E_{\rm tot}$ is the sum of the energy in the fermions and in the classical Bose fields,

$$E_{\rm tot}(t) = E_b(t) + E_f(t), \qquad E_b(t) = \sum_x \left[\tfrac{1}{2}e^2E^2(x,t) + |\pi(x,t)|^2\right] + V_{\rm pot}(t), \tag{6.12}$$

with

$$e^2E(x,t) = \partial_0 A_1(x,t), \qquad \pi(x,t) = \partial_0\phi(x,t),$$
$$V_{\rm pot}(t) = \sum_x \left[|D_1\phi(x,t)|^2 + \lambda\left(|\phi(x,t)|^2 - v_B^2/2\right)^2\right].$$

Let us conclude this section with the following remarks. When the initial state of the system is homogeneous, the system will remain homogeneous during the time evolution. The space dependence of the mode functions is given by plane waves for all times, and there is no mode mixing. The equations of motion reduce to ordinary differential equations. In the case of inhomogeneous initial conditions, the subsequent space dependence is determined by the equations. There is mode mixing, and the label p loses its interpretation for $t > 0$. Since the initial state of the fermions we use here, is chosen to be homogeneous, the inhomogeneity in the initial conditions has to be put into the Bose fields. This should be done in such a way that the total Higgs charge is zero, $Q_h(0) = 0$ (since $Q_f(0) = 0$) and that it does not violate the local Gauss' law (6.2). In this one space-dimensional model, this can be done in a straightforward manner. Another possibility to introduce inhomogeneity would be to start not with a plane wave basis for the fermions, but with wave packets. This could be used to study

scattering between fermions. This would correspond to an initial density matrix that is not quadratic in the fermion field.

Before diving into the full dynamics, we first analyse the response of the fermions to certain external Bose field configurations.

7. Handmade sphaleron transitions

In the previous section, we listed the effective equations of motion and the initial conditions for the fermion mode functions. Once the initial Bose fields are specified, the equations can be solved (numerically). In order to gain experience with the equations for the mode functions, we treat in this section the Bose fields as *external* fields. We focus on sphaleron transitions: the Bose fields start in a vacuum configuration, characterized by a certain integer Chern–Simons number C and scalar field winding number n, go through a sphaleron, and end up in a vacuum where C and n have changed by one unit. This analysis is closely related to the spectral flow analysis, which we summarize in Appendix C. However, when considering spectral flow, usually the Dirac Hamiltonian is diagonalized for every external Bose field configuration [22,17]. Here we use the real-time approach and solve the equations of motion for the mode functions in the presence of the Bose fields. Such a calculation can be done analytically in the case of QED with a homogeneous gauge field [23]. We do not have to discuss renormalization of the effective equations of motion at this stage, since the Bose fields are external, and the divergence is only present in the fermion back reaction. The divergence in the fermion energy is renormalized as in (6.11). We stress again that the main purpose of this section is to test the equations for the mode functions.

The Bose configurations we use are the following. A vacuum configuration with Higgs winding number n is given by

$$\phi_n = \frac{v}{\sqrt{2}} \exp\left(2\pi i n \frac{x}{L}\right) = \frac{v}{\sqrt{2}} V_n.$$

Note that on the lattice n is only defined modulo N, because $Nx/L = x/a$ is integer. We use the gauge invariant definition of the winding number [24] on a periodic lattice,

$$\begin{aligned} &\phi(x,t) = \rho(x,t) e^{i\theta(x,t)}, \\ &n(t) = \frac{1}{2\pi} \sum_x \Big([\theta(x+a,t) - \theta(x,t) - A_1(x,t)]_\pi + A_1(x,t) \Big), \\ &[f]_\pi = f \,(\mathrm{mod}\, 2\pi) \in (-\pi, \pi]. \end{aligned}$$

The corresponding gauge field configuration is

$$A_1^n = \frac{2\pi n}{L}, \qquad C = -n.$$

The sphaleron configuration is given by

$$\phi_s = -\frac{v}{\sqrt{2}} \tanh\left(\sqrt{\lambda/2} v(x - L/2)\right) \exp\left(i\pi \frac{x}{L}\right), \qquad A_1 = -\frac{\pi}{L}, \qquad C = \tfrac{1}{2}.$$

We go from one vacuum to another through the sphaleron in a time t_0, with the sphaleron being halfway. t_0 sets the time scale. Since we want to go through several vacua after each other, the configurations are taken to be ($t' = t/t_0$)

$$\phi(t') = f(t')\phi_{n_v} + (1 - f(t'))\phi_s V_{n_s}, \qquad A_1(t') = \frac{2\pi}{L} g(t'),$$

where the winding number n_v changes from n_v to $n_v + 1$ at t' being half-integer, and n_s from n_s to $n_s + 1$ at t' being integer. At $t' = 0$, $n_v = n_s = 0$. The profile functions f, g that determine the time-dependence obey the following conditions: f equals 1 at integer t', and 0 at half-integer t', and g equals t' at (half-)integer t'. Furthermore, we require the time derivatives of f, g to vanish at t' being (half-)integer.[7] This means that the configuration is 'stationary' both on top of the sphaleron and in the ground state. Note that these configurations are inhomogeneous in general.

The parameters we use in this section are

$$\begin{aligned} &N = 32, \quad a_0/a = 0.05, \quad eL = 3.2, \quad et_0 = 2, \\ &v^2 = 4, \quad \lambda/e^2 = 0.25, \quad G/e = 0.1, \end{aligned} \tag{7.1}$$

except when indicated otherwise. Let us shortly discuss the lattice spacing dependence. All the results we present are for a fixed physical size eL. Hence, increasing the number of lattice points N reduces in fact the lattice spacing a. Furthermore, the time scale $et_0 = 2$ we take here is sufficiently large such that all physical time scales are large compared to lattice scales, but also not so large that the adiabatic approximation ($et_0 \to \infty$) tells all.

In Fig. 2, we show a characterization of the Bose fields configuration, i.e. the Chern–Simons number, the winding number, and the potential energy in the Bose fields, normalized with the sphaleron energy. The potential energy in the Bose fields is the well-known periodic potential.

In Fig. 3 we show the response of the fermions, i.e. the change in the axial charge, when going through the series of configurations of Fig. 2. The axial charge follows the Chern–Simons number, which changes from 0 to 4. This is the anomaly equation. There are high frequencies oscillations present in Q_5, which are more clear in Fig. 4, where we show a blow up of Fig. 3 for two values of the lattice spacing in time, $a_0/a = 0.1, 0.05$. These high frequency oscillations reflect that the lattice Dirac equation is a three term difference equation in time. Indeed, in the case of the free Dirac equation we find the solutions

$$\Psi(x,t) = e^{ipx - i\omega t}\Psi_{p\omega}, \qquad \omega = \pm E_p, \qquad \omega = \frac{\pi}{a_0} \mp E_p.$$

The first solution represents the normal physical particles, the second solution is the sum of a high frequency part ($\propto 1/a_0$) and a low energy part representing the doubler.

[7] To be explicit, we use $f(t') = \cos^2 \pi t'$, $g(t') = t' - (4\pi)^{-1} \sin 4\pi t'$.

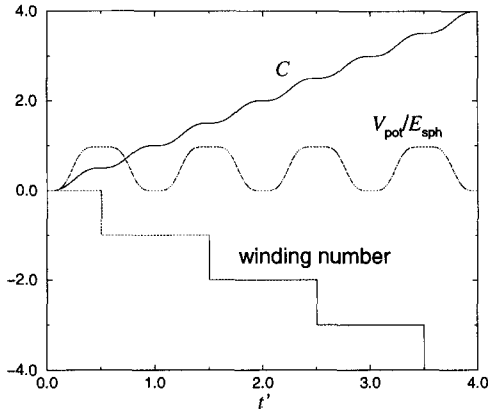

Fig. 2. Characterization of the Bose fields configuration: the Chern–Simons number, the Higgs winding number and the potential energy in the Bose fields, normalized with the sphaleron energy, versus t', for parameters (7.1).

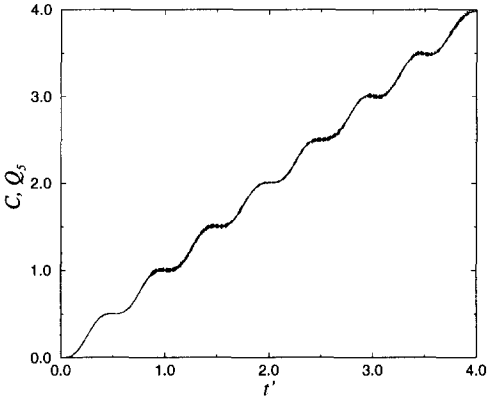

Fig. 3. Response of the fermions: the axial charge Q_5 (solid, with rapid oscillations) and the Chern–Simons number C (dotted) versus t', for several sphaleron transitions, $C = 0 \rightarrow 4$. The lines fall mostly on top of each other, in accordance with the anomaly equation. Parameters as in (7.1).

The high frequency part gives a $(-1)^{t/a_0}$ behaviour with an amplitude that vanishes as a_0^2.

Like the axial charge, the fermion energy has rapid oscillations, with an amplitude that decreases for increasing a_0. The energy transferred to the fermions and the sum of the fermion and the potential energy in the Bose fields is presented in Fig. 5. We use here a very small $a_0/a = 0.005$ to suppress the rapid oscillations. The fermions lift the degeneracy of the bosonic ground state, and introduce local minima. The picture is symmetric for $C \rightarrow -C$ $(t' \rightarrow -t')$, we have no CP violation in our model.

We would like to stress that taking the doublers into account leads to a consistent time evolution. One can imagine to start with only the mode functions for the normal particles. Let us recall that these are initialized as smoothly as possible, $U_{\alpha u}(x,0) = U_{\alpha u}(x,a_0)$. Right after $t = 0$, only the normal particles are present. However, due to the non-linearity

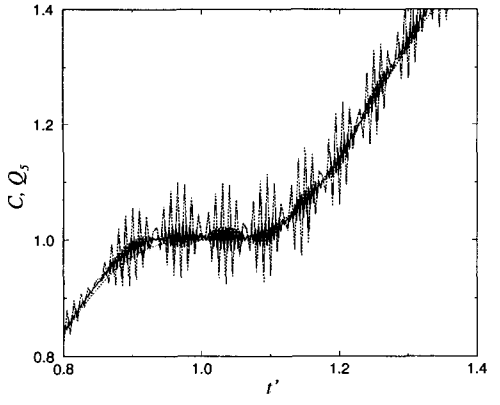

Fig. 4. As in Fig. 3. Blow-up showing C (dotted, slowly varying) and Q_5 with rapid oscillations $\propto a_0^2(-1)^{t/a_0}$ due to the time discretization, for two values of the lattice spacing in time, $a_0/a = 0.1$ (larger amplitude) and 0.05 (smaller amplitude).

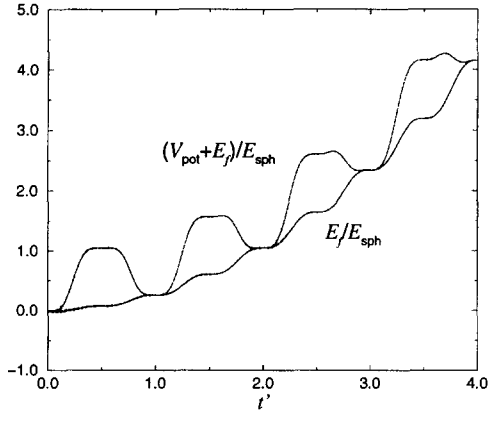

Fig. 5. Energy of the fermions and the sum of the energy of the fermions and the potential energy in the Bose fields, normalized with the sphaleron energy, versus t'. Parameters as in Fig. 3, with $a_0/a = 0.005$.

of the equations of motion, high frequencies will be generated, and in order to make sense out of these, the doubler interpretation has to be introduced after all. Hence, it is better to include them from the start. In terms of evolution in Hilbert space, including the doublers explicitly leads to unitary time evolution in the Hilbert space that is associated with the lattice path integral.

Another test is the periodicity of Q_5 on the lattice. As explained in Appendix C for vanishing Yukawa coupling, if $C = N(-N)$ the axial charge takes its maximal (minimal) value, and if $C = \pm 2N$, the total axial charge is zero again. Although this phenomenon is a lattice artefact, which is due to the finite number of states, it still serves as a check on the fermion system. We show the outcome of this test in Fig. 6 for $N = 16, 32$ and $G/e = 0$. Plotted are Q_5/N versus t'/N, because the curves should then fall on top of each other for large N. We see this to be the case already for these small N values. The maximum Q_5 also agrees well with the value $2/\pi \approx 0.637$ for

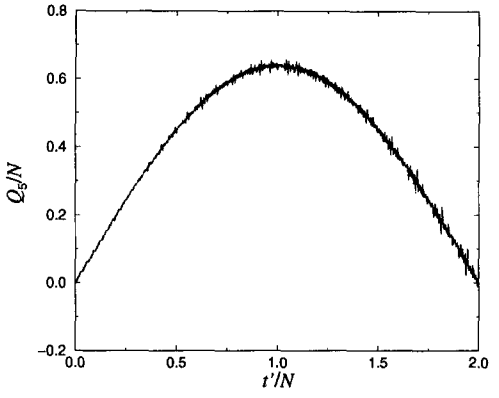

Fig. 6. Lattice periodicity of Q_5 for zero Yukawa coupling: Q_5/N versus t'/N for two values of the lattice spacing, $N = 16, 32$. After the rescaling with N, the lines converge to the same curve, as expected. Other parameters as in Fig. 3.

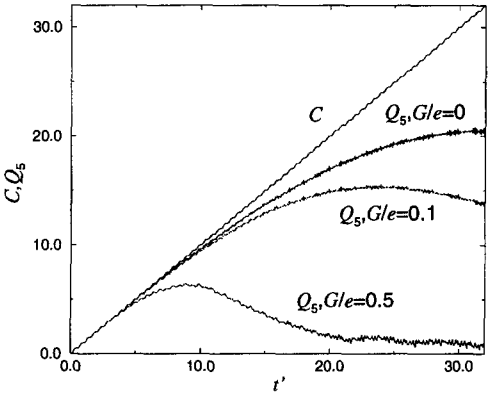

Fig. 7. As in Fig. 3, C and Q_5 for three values of the Yukawa coupling, $G/e = 0, 0.1, 0.5$. For larger Yukawa couplings, lattice artefacts are more important.

$N \to \infty$ (cf. (C.4)). Of course, this maximum is way out of the region where there is continuum behaviour, i.e. where the anomaly equation is satisfied ($Q_5 \approx C \approx t'$), which appears to be $|Q_5|$ smaller than $N/4$.

We proceed with an investigation of the effect of a finite Yukawa coupling. In Fig. 7, we show the behaviour of the axial charge for three values of the Yukawa coupling, $G/e = 0, 0.1, 0.5$, up to a large Chern–Simons number $C = N$. In the continuum regime $|Q_5| \lesssim N/4 = 8$, the anomaly equation is (approximately) satisfied for finite G as well, but the deviation of Q_5 from C becomes more and more important for larger G. This can be further investigated by taking a fixed finite coupling $G/e = 0.1$, and decreasing the lattice spacing (increasing the number of lattice points). The result is shown in Fig. 8, for $N = 16, 32, 64$. We conclude that for a finite Yukawa coupling lattice artefacts are more important, and that for fixed Yukawa coupling, an increase in the number of lattice points shows convergence to the continuum limit. It is also known from previous (lattice) studies (see e.g. Ref. [22]) that a finite Yukawa coupling has a relatively large

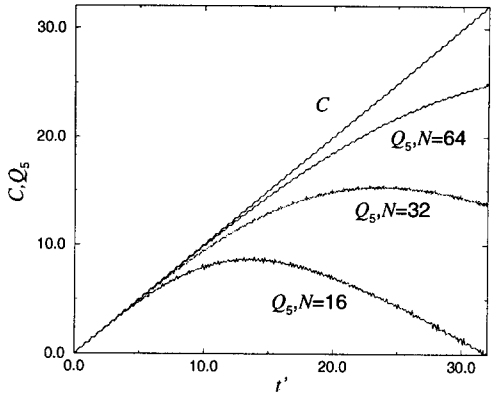

Fig. 8. As in Fig. 3, C and Q_5 for fixed Yukawa coupling, $G/e = 0.1$, and three values of the lattice spacing, $N = 16, 32, 64$. Decreasing the lattice spacing (increasing N) shows convergence to the continuum limit.

influence on the relation between the anomalous charge and the Chern–Simons number.

Summarizing the results obtained in this section, we found that using a controlled series of external Bose fields configurations, the system behaves for zero and small Yukawa couplings as expected. For bigger Yukawa couplings, the lattice artefacts are substantially larger. With this in mind, we can continue and study the complete dynamics.

8. Renormalization

We go on with the full dynamics, and include the back reaction. The full quantum theory contains ultraviolet divergences, which are regulated by the lattice cutoff. In this section, we discuss the renormalization and show numerical results to demonstrate its applicability.

Let us first make some remarks about the role of the parameter v^2. By rescaling according to

$$\phi = v\phi', \qquad e = e'/v, \qquad G = G'/v \qquad \lambda = \lambda'/v^2, \tag{8.1}$$

v^2 appears in front of the bosonic part S_B of the effective action, with the fermionic part $-\frac{1}{2}i\log D$ unchanged. Hence, if we also scale the bosonic initial conditions accordingly, the influence of the fermions is scaled by a factor $1/v^2$, and the fermion back reaction gets reduced at larger v^2. This can also be seen directly from the effective equations of motion.[8] This is of course not surprising since $1/v^2$ is indeed the dimensionless semiclassical expansion parameter.

As indicated in Section 2, only the scalar self-energy is divergent in the full quantum theory. The divergence is renormalized by the appropriate choice of v_B^2. Therefore, let us take a closer look at the equation for the scalar field (6.3). Because we treat the Bose fields as classical and only the fermions are integrated out, we expect to find only the

[8] To be precise, the rescaling is with a finite $v = v_R$, this introduces a rescaled bare $v_B' = v_B/v_R$.

fermion one-loop divergence of the Higgs self-energy. To see this explicitly, we consider for simplicity a ground state configuration for the Bose fields, $A_1 = 0$, $\phi = v_R/\sqrt{2}$, where v_R is the renormalized, effective Higgs expectation value. Substituting this in (6.3), gives the gap equation

$$\lambda(v_R^2 - v_B^2)\frac{v_R}{\sqrt{2}} = G\langle F\rangle(v_R), \tag{8.2}$$

where we indicated that the mode functions are initialized with $v = v_R$. Using (6.10) for $\langle F\rangle(v_R)$, we see that it depends on Gv_R through $m_{p\eta}$ and $E_{p\eta}$. This makes (8.2) a highly non-linear equation in G and v_R. We can, however, perform a lowest order approximation, and expand the right-hand side in G, to find (at zero initial temperature $\sigma_{p\eta f} = 1$)

$$\langle F\rangle(v_R) = \frac{Gv_R}{\sqrt{2}}\frac{1}{L}\sum_p \frac{1}{E_{p0}}\left(1 - \frac{m_p^2}{E_{p0}^2}\right) = \frac{Gv_R}{\sqrt{2}}\left(\frac{1}{\pi}\log N + \mathcal{O}(N^0)\right),$$

where E_{p0} is independent of Gv_R. The sum contains the expected logarithmic divergence, which we indicated as $\log N$. Using this approximation, the gap equation (8.2) has two solutions

$$v_R = 0, \qquad v_R^2 = v_B^2 + \frac{G^2}{\lambda}\frac{1}{L}\sum_p \frac{1}{E_{p0}}\left(1 - \frac{m_p^2}{E_{p0}^2}\right).$$

The log divergence in the second solution is cancelled with v_B^2.

In practice, we fix v_R^2 and then find (for certain N) the corresponding bare parameter v_B^2, simply from (8.2),

$$v_B^2 = v_R^2 - \frac{G}{\lambda}\frac{\sqrt{2}}{v_R}\langle F\rangle(v_R), \tag{8.3}$$

with $\langle F\rangle$ given by (6.10). We demonstrate this with numerical results. We use the following parameters:

$$\begin{array}{lll} N = 16, 32, 48, & a_0/a = 0.1, & eL = 3.2, \\ v_R^2 = 11.15 & \lambda/e^2 = 0.25, & G/e = 0.5, \end{array} \tag{8.4}$$

and as initial Bose fields configuration, we take

$$\begin{aligned} &\phi(x,0) = \frac{v_R}{\sqrt{2}}, \qquad \partial_0\phi(x,0) = 3e\cos\frac{2\pi x}{L}, \\ &A_1(x,0) = 0, \qquad \partial_0 A_1(x,0) = \text{Gauss' law} + e^2. \end{aligned} \tag{8.5}$$

We start with a slowly varying wave for $\partial_0\phi$. The space dependence of $\partial_0 A_1$ is determined by Gauss' law (6.2) (it is zero in this simple case), only the homogeneous part can be freely chosen (it is the 'conjugate variable' for the Chern–Simons number degree of freedom). Note that for this type of initial conditions, the initial energy of the whole system is entirely in Bose fields with long wave lengths.

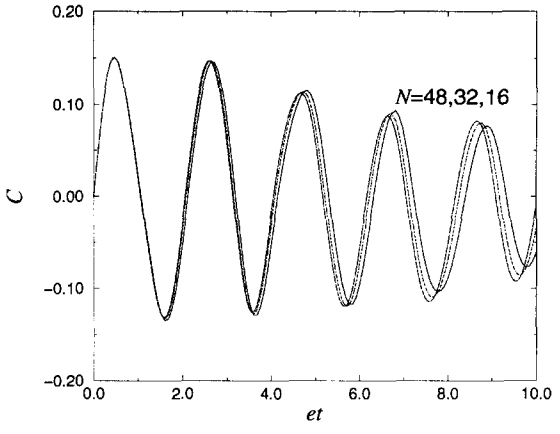

Fig. 9. Need for renormalization: Chern–Simons number C versus et for fixed bare v_B, for three values of the lattice spacing, for parameters (8.4) and initial conditions (8.5). The lines show dependence on the lattice spacing.

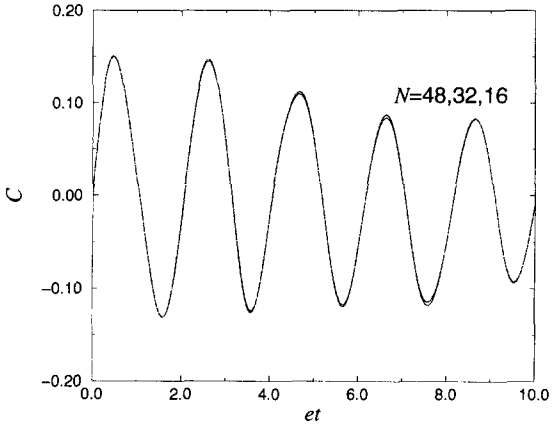

Fig. 10. Renormalization: as in Fig. 9, C versus et for fixed renormalized v_R, and three values of the lattice spacing. The bare parameter v_B is determined from (8.3). The line with largest lattice spacing ($N = 16$) shows the largest discrepancy, and convergence towards the continuum limit is clearly visible.

In Fig. 9, we show the Chern–Simons number as a function of time for three values of the lattice spacing ($N = 16, 32, 48$). C undergoes a damped oscillation. The bare expectation value is kept fixed, $v_B^2 = 10$, and *not* changed according to (8.3). The three curves do not agree, and the period is lattice spacing dependent. In Fig. 10, we perform the same calculations, but now with a fixed renormalized expectation value, $v_R^2 = 11.15$. The bare expectation value that enters in the dynamics is determined according to (8.3), and is N dependent. The value of v_R is chosen in such a way that for $N = 48$, $v_B^2 = 10$, such that the curves can be compared with the $N = 48$ curve in Fig. 9. In this case, we see that the three lines fall on top of each other, and there is convergence towards the physical continuum limit. The line that shows the largest discrepancy is for largest lattice spacing ($N = 16$).

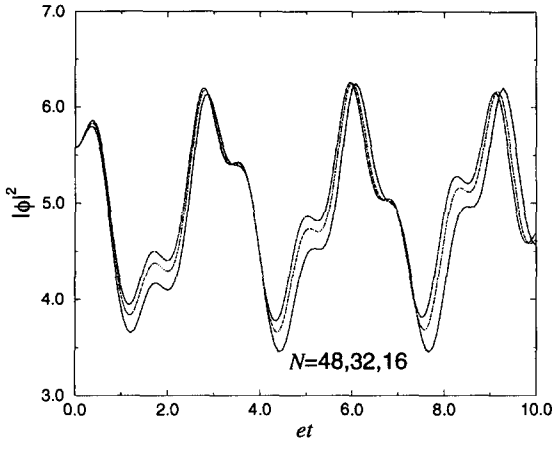

Fig. 11. Need for renormalization: as in Fig. 9, the scalar field amplitude $|\phi|^2$ versus et, for fixed bare v_B, and three values of the lattice spacing. Again there is lattice spacing dependence.

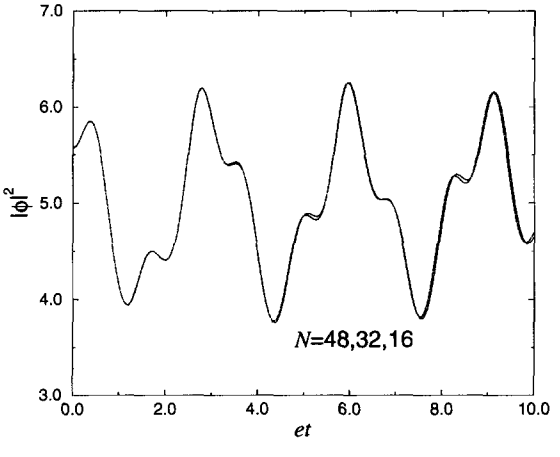

Fig. 12. Renormalization: as in Fig. 11, $|\phi|^2$ versus et, for fixed renormalized v_R, and three values of the lattice spacing. The lines show a quick convergence towards the continuum limit, the lines with $N = 32, 48$ are already indistinguishable.

To show that the observed convergence is also true for other observables, we repeat the analysis for $|\phi|^2 = L^{-1} \sum_x |\phi(x,t)|^2$. In Fig. 11, v_B^2 is kept fixed, and the curves show again lattice spacing dependence. In Fig. 12, we keep again v_R^2 fixed, and determine v_B^2 according to (8.3). Again this leads to converging physical results, with the largest discrepancy for smallest N, $N = 16$.

We conclude that there is no convergence when the bare parameters are not adapted in the proper way, i.e. according to (8.3). A correct renormalization leads to convergence towards the physical continuum limit, already for fairly small N.

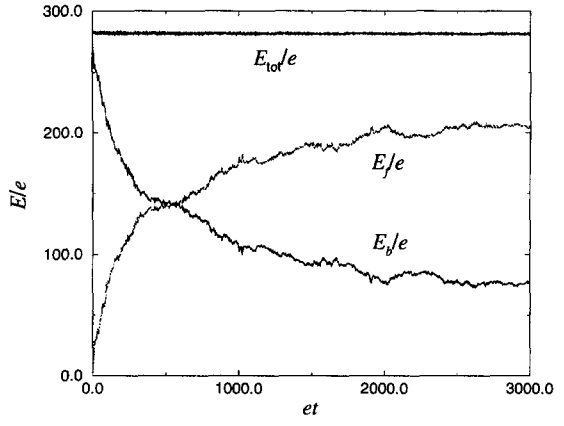

Fig. 13. Non-perturbative dynamics: energy of the Bose fields E_b/e, the fermion field E_f/e, and the sum $E_{\rm tot}/e$ versus et, for initial conditions (9.1) and parameters (9.2) with $v_R^2 = 8, G/e = 0$.

9. Non-perturbative dynamics

In the previous section, the total energy of the system was, in some sense, not very large. The Chern–Simons number simply oscillates around zero, with an amplitude which is not larger than 0.2. There are no sphaleron transitions, C does not get larger than 0.5. In this section we consider systems with more energy.

To achieve this, we use the same type of initial Bose fields configurations as in the previous section, but with two wave lengths and complex amplitudes

$$\begin{aligned} &\phi(x,0) = \frac{v_R}{\sqrt{2}}, \qquad \partial_0\phi(x,0) = 6e(1+i)\cos\frac{2\pi x}{L} + 2e(1+2i)\cos\frac{4\pi x}{L}, \\ &A_1(x,0) = 0.1/L, \qquad \partial_0 A_1(x,0) = \text{Gauss' law} + e^2. \end{aligned} \tag{9.1}$$

The parameters are

$$\begin{aligned} &N = 32, \quad a_0/a = 0.05, \quad eL = 3.2, \\ &v_R^2 = 8(4), \quad \lambda/e^2 = 0.25, \quad G/e = 0.0(0.1). \end{aligned} \tag{9.2}$$

We begin with the case of zero Yukawa coupling. The fermions start in a vacuum state, with zero energy. All the initial energy is in the Bose fields. We show the energy in the Bose fields E_b, in the fermion field E_f and the total energy $E_{\rm tot}$ in Fig. 13, for fairly larger times than in the previous section, $0 < et < 3000$. The total energy is conserved up to small oscillations, very similar to the result from a leapfrog algorithm. The initial state is clearly a non-equilibrium situation, and there is energy transfer from the Bose fields to the fermion degrees of freedom. Presumably there is fermion particle production, as in the non-equilibrium homogeneous models studied before [4–9].

In Fig. 14 we show the Chern–Simons number and the axial charge. Initially, there is a lot of energy present in the Bose fields. The Chern–Simons number is wildly moving. The Bose system does not feel the sphaleron energy barriers. However, there is continuous energy transfer towards the fermions, and plateaus become visible. The

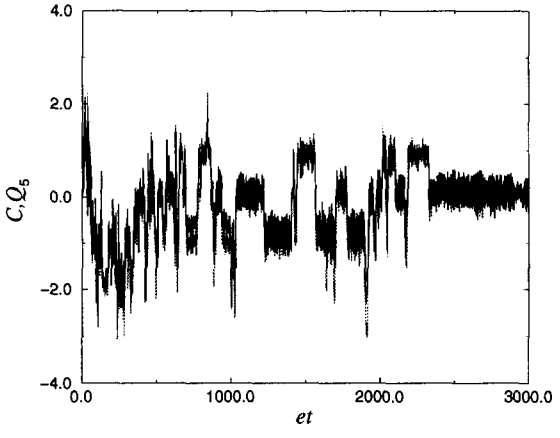

Fig. 14. As in Fig. 13, Chern–Simons number C (dotted) and axial charge Q_5 (solid) versus et. The lines cannot always be distinguished, which is in accordance with the anomaly equation. Small deviations, e.g., around $et \approx 1300$, are due to the finite lattice spacing.

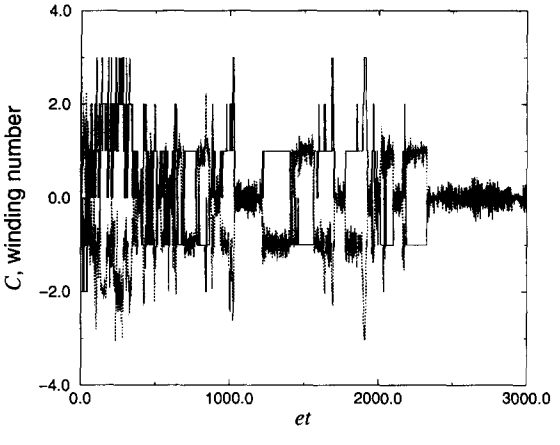

Fig. 15. As in Fig. 13, Chern–Simons number C (dotted) and Higgs winding number (solid) versus et. The lines are anticorrelated, which is expected when sphaleron transitions dominate.

energy transfer continues and the time the system spends in one 'vacuum' becomes longer. Q_5 follows C, and it is not always possible to distinguish Q_5 from C. This is actually a nice property, because it shows that the anomaly equation is correctly reproduced. Small differences are due to the finite lattice spacing. In Fig. 15 we show the Chern–Simons number and the Higgs winding number. The winding number is anticorrelated with C when sphaleron transitions dominate, as expected from Section 7.

Let us this stage discuss the stability of the numerical algorithm. The total charge $Q = Q_f + Q_h$ is conserved better than $\mathcal{O}(10^{-10})$ (actually, for zero Yukawa coupling, both Q_f and Q_h are separately conserved). The first component of the vector triplet charge $Q_{\mathfrak{fl}}$ is conserved better than $\mathcal{O}(10^{-16})$. Locally, Gauss' law is respected better than $\mathcal{O}(10^{-10})$.

For finite Yukawa coupling, we found in Section 7 with the help of handmade

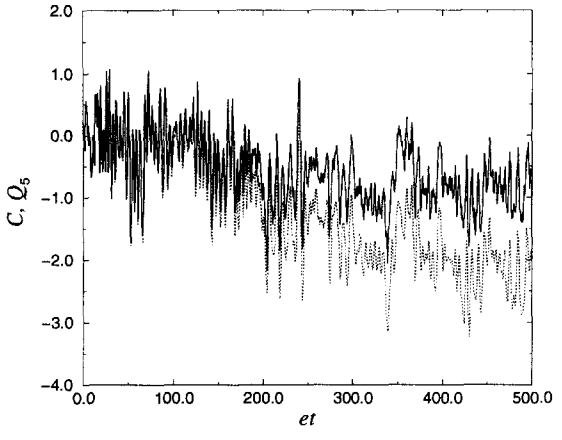

Fig. 16. As in Fig. 13, Chern–Simons number C (dotted) and axial charge Q_5 (solid) versus et, for finite Yukawa coupling $G/e = 0.1$, and $v_R^2 = 4$. After a finite time, Q_5 loses C, and the anomaly equation is no longer satisfied.

sphaleron transitions, that the axial charge is more sensitive to the lattice discretization. In particular, for the typical parameters used in this section and with $N = 32$, the axial charge suffers quite a lot from discretization effects. This indeed shows up in the dynamics. In Fig. 16 we show C and Q_5 for $v_R^2 = 4, G/e = 0.1$ and et between 0 and 500. The anomaly equation is reasonably satisfied only for a finite time, in contrast to the $G/e = 0$ example.

10. Finite temperature and density

Let us summarize what we have done so far. In all the results we have shown, the initial Bose fields are long wave length fields. The fermion contribution is calculated starting from a vacuum state, i.e. (6.7) with $T_{f,\mathrm{in}} = 0$. It is straightforward to start with a non-zero fermion temperature, and study e.g. the effect of (Landau) damping on the Bose fields due to a thermal bath of fermions.

However, in this section we would like to comment briefly on the possibility of applying the methods used in this paper to a situation where also the Bose fields are thermal. Such a system would describe a thermal plasma consisting of classical Bose fields and quantum fermion fields. This would be interesting e.g. from the perspective of baryogenesis.

In this situation, there are several cases to be distinguished: either the initial state of the system may be prepared according to a typical equilibrium configuration, or the initial state of the system is prepared out of equilibrium, but it reaches some sort of equilibrium at large times.

The first situation implies that it is known what a typical equilibrium situation looks like. One might think that it may be approximately realized as follows. Choose a temperature T in the Fermi–Dirac distribution (6.7) specifying the fermion initial conditions.

Prepare the Bose fields in a classical equilibrium configuration at this temperature, i.e. draw them from the classical canonical distribution $\exp(-E_b/T)$. Correlation functions are then computed by averaging over such initial configurations. Note that in this way one has prepared two subsystems which are *separately* in equilibrium, i.e. the Bose and the fermion subsystem, and that these are coupled together at $t > 0$. If the theory is weakly coupled, and the back reaction of the fermions is perturbative, this can be analyzed using perturbation theory, along the lines as in 3+1 [25,26] and 1+1 [12] dimensions for a purely classical Bose system. In the classical theory (without the fermions), perturbation theory leads to the conclusion [12] that the classical approximation is good[9] in 1+1 dimensions, for $T = v^3\sqrt{\lambda}T'$, with $v^2 \gg 1$ (cf. (8.1)) and $T' = O(1)$. If the fermions are included, we should be able to reproduce numerically this way the fermion and boson propagators calculated analytically in the one-loop approximation in the appropriate momentum and frequency regime.

However, an actual numerical implementation of this idea leads us to the conclusion that for times beyond the validity of the perturbative calculation, the fermion back reaction becomes non-perturbative and the *coupled* system is in fact still far from equilibrium.

The other possibility, the system is initialized in a non-equilibrium state, but reaches some sort of equilibrium at large times, relies on the assumption that the effective equations of motion are chaotic in the relevant coarse grained variables, such that at large times they lead to a distribution (by averaging over time) that approximates the microcanonical ensemble of the original quantum system. At present it is not known to us if this assumption is correct in some sense. We hasten to say that the objection raised sometimes to the effective equations that they do not incorporate scattering and therefore do not lead to the desired equilibrium distribution, is misleading in the inhomogeneous case considered here. One can easily convince oneself that there is non-trivial scattering in the effective equations, e.g. by taking an initial state of two fermion wave packets approaching each other: the localized fermions will simply experience approximately classical Coulomb scattering.

Still, it is a deep fundamental question what happens at large times, in the original system, and in the effective field equations, given for example initially a bosonic configuration with a certain energy and a fermions initialized in a vacuum or thermal state.

Here we only provide one numerical example to show the very long time behaviour. In Fig. 17 we show the fermionic and bosonic energies, for initial Bose fields as in the previous section, i.e. (9.1), and also a similar choice of parameters

$$N = 32, \quad a_0/a = 0.1, \quad eL = 3.2,$$
$$v_R^2 = 8, \quad \lambda/e^2 = 0.25, \quad G/e = 0.1.$$

[9] In the sense of the absence of ultraviolet divergences in classical thermal loops and the agreement with the results from high temperature quantum field theory.

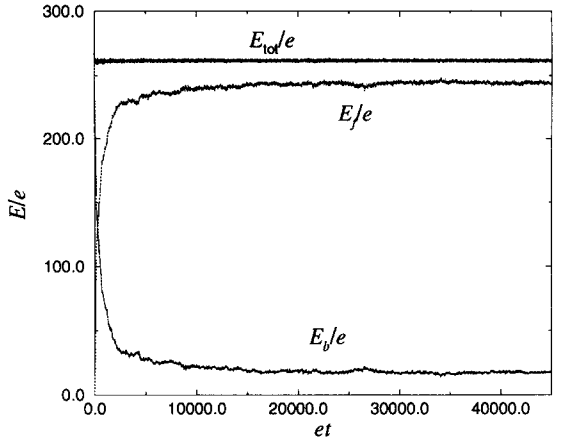

Fig. 17. Long time behaviour, energies versus et. Initial conditions and parameters as in Fig. 13, except that $G/e = 0.1$.

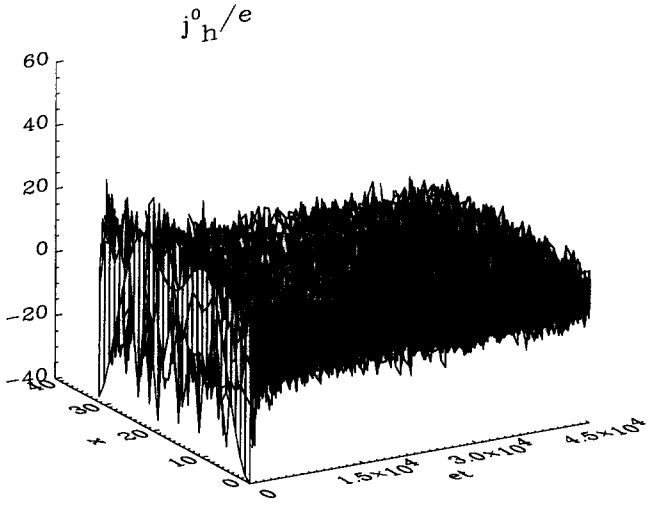

Fig. 18. As in Fig. 17, charge density of the scalar field $j^0_h(x,t)/e$ versus x/a and et.

Notice, however, that the time interval $0 < et < 45000$ here is 15 times as large as in the previous section ($0 < et < 3000$). The system is evidently initially quite out of equilibrium, while at larger times the bosonic energy only drops very slowly. The bosonic energy drops by a factor of more than 15 as it gets transferred to the fermions. This may be related to our neglect of the bosonic fluctuations. To visualize the effect of decreasing bosonic energy in a typical bosonic observable, we show in Fig. 18 the charge density of the scalar field as of function of space x (in lattice units, $x/a \in \{0, \ldots, N-1\}$) and time et. Note that initially the size of the amplitudes decreases, but then remains approximately of the same size. Furthermore the system remains fluctuating, and inhomogeneous. More detailed analysis is needed to determine if the end result is approximately thermal in the quantum sense.

If the system does thermalize in a reasonable way we have an approximate non-perturbative method for computing at finite temperature. An application would be e.g. the thermal sphaleron rate in the presence of CP-violating fermions. Last, but not least, the same would apply to finite density. It is not difficult to prepare an initial state with a non-zero conserved quantum number (e.g. $Q_{\rm fl}$ defined in Section 3). The corresponding finite density microcanonical ensemble could then emerge at large times. It would provide a new approach to the problem of non-perturbative finite density computations in QCD.

11. Summary and outlook

We considered a coupled system of classical Bose fields and a fully quantized fermion field, to approximate non-perturbative real-time dynamics in quantum field theory. The fermion back reaction was computed using a mode function expansion, similar to previous work in the homogeneous case. However, these mode functions still contain the full space dependence and this makes the numerical problem scale like N^{2d+1} in d space dimensions. The immediate consequence is that the calculation of the back reaction is numerically much more demanding than in the homogeneous situation. The 1+1-dimensional model served as a useful laboratory for testing.

The lattice discretization leads to fermion doubling, which is well-known in Euclidean lattice gauge theory. We added a Wilson term in space to deal with the space doublers, but used 'naive fermions' in time. The time doublers were interpreted as a second flavour. In hindsight the treatment of fermion doubling could perhaps be done in a more elegant way, e.g. using staggered fermions, which might also lead to smaller discretization errors.

We have studied several dynamical questions with the effective equations of motion. First we used external time dependent Bose fields to test the treatment of the fermions, using the mode functions. We found that the anomaly equation relating the anomalous charge and Chern–Simons number is correctly reproduced. However, for a finite Yukawa coupling discretization errors are larger and qualitatively different in the sense that the anomalous charge loses Chern–Simons number after some time. This time increases with decreasing lattice distance.

Next we studied the quantum divergence which is present in the effective equations of motion and we showed how this can be renormalized. We then demonstrated the applicability of the approximation to non-equilibrium time evolution on a few initial value problems. Finally, we have discussed the possibility that the effective dynamics can be used to describe a plasma at finite temperature and density. We have shown some preliminary results at very long times which indicated equilibration to an ensemble of (inhomogeneous) configurations.

Possible directions for the future are many. CP violation can be incorporated by extending the model with more fermion fields, relevant for baryogenesis. Analytical calculations of various damping mechanisms of Bose fields due to a thermal bath of fermions

can be checked numerically. In the typical examples we have shown, there is a large energy transfer from the Bose fields to the fermion fluctuations, as in inflationary scenarios. This energy transfer can presumably be interpreted as particle production, using the idea of adiabatic particle numbers. An analysis of this would require a space dependent Bogoliubov transformation. All of this is on reasonably firm theoretical grounds. Concerning the long time behaviour, and the possible approach to (some) equilibrium, we would like to stress that many questions are still open and require a detailed study.

A big issue is of course how to extend this approach to 3+1 dimensions. Brute force using all the mode functions seems hopeless, but useful inspiration can perhaps be found in the dynamical fermion methods used in four-dimensional Euclidean lattice QCD. It should of course also be kept in mind that the ultraviolet properties of classical gauge fields in thermal equilibrium are different in $3+1$ dimensions than in $1+1$ dimensions.

Acknowledgements

It is a pleasure to thank Gerard Barkema and Bert-Jan Nauta for useful discussions and comments. This work is supported by FOM.

Appendix A. Dirac matrices, Dirac and Majorana spinors

Our conventions are the following. The Dirac matrices obey $\{\gamma^\mu, \gamma^\nu\} = g^{\mu\nu}$, with $-g^{00} = g^{11} = 1$. The antisymmetric Levi-Civita tensor $\epsilon^{\mu\nu}$ is defined by $\epsilon_{01} = 1$. $\gamma_5 = -\gamma^0\gamma^1$. The charge conjugation matrix obeys $\mathcal{C}^\dagger = \mathcal{C}^{-1}, \mathcal{C}^T = -\mathcal{C}$, and $\mathcal{C}\gamma^{\mu T}\mathcal{C}^\dagger = -\gamma^\mu$, and hence

$$\mathcal{C}{\gamma_5}^T\mathcal{C}^\dagger = -\gamma_5, \quad \mathcal{C}P_{L,R}^T\mathcal{C}^\dagger = P_{R,L},$$

which is different than in $3+1$ dimensions. We also use the hermitian matrices $\alpha^1 = -\gamma^0\gamma^1, \beta = i\gamma^0$. The adjoint spinor is $\bar{\psi} = \psi^\dagger\beta$.

As explicit representation we use the Majorana–Weyl representation $\gamma^0 = -i\sigma_2, \gamma^1 = \sigma_1, \gamma_5 = \sigma_3$, and $\mathcal{C} = \beta$.

Working on the lattice with Wilson fermions, the following combination often appears

$$P_\pm^\mu = \tfrac{1}{2}(r_\mu \pm \gamma^\mu).$$

In this paper we restrict ourselves to $r_0 = 0$.

Finally, Pauli matrices acting on the 1,2 components of a Majorana spinor are denoted with $\rho_{1,2,3}$ and Pauli matrices acting in flavour space with $\tau_{1,2,3}$.

Appendix B. Eigenspinors in a vacuum background

In this paper we take as initial mode functions the eigenspinors of the Dirac Hamiltonian in a vacuum background of Bose fields, i.e. $\phi = v_R/\sqrt{2}, A_1 = 0$. In this case the

eigenspinors can be found analytically, by spatial Fourier transformation.

The Dirac Hamiltonian (3.17) in a vacuum background is given by

$$\mathcal{H}_{D\!\!\!/p} = \alpha^1 s_p + \beta(m_p + \rho_3\tau_3 m_F), \tag{B.1}$$

with $s_p = a^{-1}\sin ap$, the spatial Wilson mass $m_p = a^{-1}r_1(1-\cos ap)$, and $m_F = Gv_R/\sqrt{2}$. ρ_3 acts on the Majorana components, and τ_3 acts in flavour space. We use antiperiodic boundary conditions for the fermion field. This quantizes p as

$$p = \frac{2\pi}{L}(n-\tfrac{1}{2}), \quad n \in \{-\tfrac{1}{2}N+1,\ldots,\tfrac{1}{2}N\}, \tag{B.2}$$

assuming N is even. The positive energy eigenvalues are summarized by

$$E_{p\eta} = \sqrt{s_p^2 + m_{p\eta}^2}, \qquad m_{p\eta} = m_p + \eta m_F, \quad \eta = \pm.$$

η refers to the product of the eigenvalues of ρ_3 and τ_3. The mixing of the Wilson mass with the mass due to the Higgs vacuum expectation value gives a mass splitting and lifts the degeneracy.

The eigenspinors can be written conveniently using the 2-spinor

$$u_{p\eta} = \frac{1}{\sqrt{2E_{p\eta}(E_{p\eta}-s_p)}}\begin{pmatrix} m_{p\eta} \\ i(E_{p\eta}-s_p)\end{pmatrix},$$

which is normalized to one, $u_{p\eta}^\dagger u_{p\eta} = 1$.

We denote the positive energy Majorana eigenspinors, with energy $E_{p\eta}$ and flavours u, d, with $U_{p\eta u}$ and $U_{p\eta d}$. They are easily constructed,

$$U_{p+u} = \begin{pmatrix} u_{p+} \\ 0\end{pmatrix}, \quad U_{p-u} = \begin{pmatrix} 0 \\ u_{p-}\end{pmatrix}, \quad U_{p+d} = \begin{pmatrix} 0 \\ u_{p+}\end{pmatrix}, \quad U_{p-d} = \begin{pmatrix} u_{p-} \\ 0\end{pmatrix}.$$

The eigenspinors needed in the mode function expansion in Section 3 are then given by

$$\tilde{U}_{\alpha u}(x) = \frac{e^{ipx}}{\sqrt{L}}U_{p\eta u}, \qquad \tilde{U}_{\alpha d}(x) = \frac{e^{ipx}}{\sqrt{L}}U_{p\eta d}. \tag{B.3}$$

where we used the collective label $\alpha = (p,\eta)$. The initial conditions for the mode functions in Section 6 are given by (3.21).

Appendix C. Spectral flow

The idea underlying spectral flow is that the equations of motion for the fermions are solved in the presence of external fields, in the special case that these external fields are extremely slowly varying. Then it is possible to use the adiabatic theorem [27] and determine the time evolution by diagonalization of the Dirac Hamiltonian for each configuration of external fields (instead of solving the equations explicitly).

In this appendix we discuss the spectral flow analysis, for the special case of zero Yukawa coupling and a homogeneous gauge field. We use Dirac fermions, with the action (3.3) and $G = 0$. In this case the spectrum can be found analytically for each value of the gauge field. The difference with the real-time analysis in the main part of this paper, is that the spectrum is calculated instantaneously for a given gauge field configuration. Hence the time doublers do not appear. The doublers in space are lifted due to the Wilson term. We use lattice units $a = 1$ in this appendix.

Let us start with the free ($A_1 = 0$) Dirac Hamiltonian. In momentum space, it is given by

$$\mathcal{H}_{Dp} = \alpha^1 s_p + \beta m_p,$$

using the notation from Appendix B. The eigenvalues and eigenspinors are

$$\mathcal{H}_{Dp} w_{p\epsilon} = \epsilon E_p w_{p\epsilon}, \qquad E_p = \sqrt{s_p^2 + m_p^2}, \quad \epsilon = \pm,$$

with

$$w_{p\epsilon} = \frac{1}{\sqrt{2E_p(E_p - \epsilon s_p)}} \begin{pmatrix} m_p \\ i(\epsilon E_p - s_p) \end{pmatrix}, \qquad w_{p\epsilon}^\dagger w_{p\epsilon'} = \delta_{\epsilon\epsilon'}.$$

Due to the Wilson mass term, these eigenspinors are not eigenspinors of γ_5 with eigenvalues ± 1. Instead they obey

$$w_{p\epsilon}^\dagger \gamma_5 w_{p\epsilon'} = \epsilon \frac{s_p}{E_p} \delta_{\epsilon\epsilon'}, \tag{C.1}$$

where s_p/E_p lies between -1 and $+1$. The sign, however, can still be used to indicate the would-be chirality in the continuum.

The fermion field is expanded as [10]

$$\psi(x) = \frac{1}{\sqrt{N}} \sum_{p\epsilon} e^{ipx} a_{p\epsilon} w_{p\epsilon},$$

where the creation and annihilation operators obey the usual anticommutation relations

$$\{a_{p\epsilon}, a_{p'\epsilon'}^\dagger\} = \delta_{pp'} \delta_{\epsilon\epsilon'},$$

and zero for the other ones. The vacuum, i.e. the Dirac sea, is given by the non-zero expectation values

$$\left\langle a_{p+} a_{p+}^\dagger \right\rangle = \left\langle a_{p-}^\dagger a_{p-} \right\rangle = 1.$$

In Fig. C.1a we show the spectrum and the filled Dirac sea for $N = 8$. The total (bare) energy and the axial charge are given by

[10] Usually the w's and a's are renamed as $w_{p+} = u_p, w_{-p-} = v_p, a_{p+} = b_p, a_{-p-} = d_p^\dagger$.

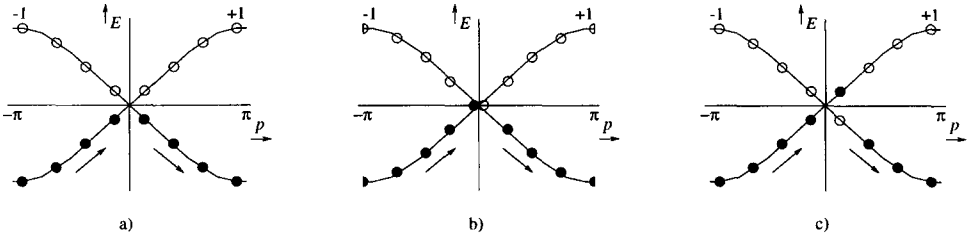

Fig. C.1. Spectrum of the Dirac Hamiltonian and distribution of occupied states on a spatial lattice with $N = 8$ sites, for (a) $C = 0$, the filled Dirac sea, (b) $C = 1$, (c) $C = 2$. The occupied states are indicated with a full dot, the empty states with a open dot. The response to an increasing Chern–Simons number is indicated with an arrow. The ± 1 denotes the sign of the γ_5 expectation value of the states on the particular branch.

$$E = \sum_x \langle \psi^\dagger \mathcal{H}_D \psi \rangle = -\sum_p E_p, \tag{C.2}$$

$$Q_5 = \sum_x \langle \psi^\dagger \gamma_5 \psi \rangle = -\sum_p \frac{s_p}{E_p} = 0. \tag{C.3}$$

The total axial charge is zero for the Dirac sea because of the precise cancellation between the + and the − branch. Because of the antiperiodic boundary conditions, there is no exact zero energy state.

The case of a homogeneous gauge field is now simply found by minimal substitution

$$p = \frac{2\pi}{N}(n - \tfrac{1}{2}) \to p - \tfrac{1}{2}A_1 = \frac{2\pi}{N}(n - \tfrac{1}{2} + \tfrac{1}{2}C),$$

where we use that the Chern–Simons number $C = -NA_1/2\pi$. Recall that the fermions have charge $q = \frac{1}{2}$. In Fig. C.1, we show the spectrum for three values of the Chern–Simons number. For $C = 1$, the spectrum is not identical to the spectrum at $C = 0$. There are now two states with exactly zero energy (one filled and one empty), and there are two states exactly at the boundary of the Brillouin zone ($p = \pm\pi$). This is not contradictory, $C + 1$ is not gauge equivalent to C, due to the $q = \frac{1}{2}$ charged fermions. $C + 2$ is gauge equivalent to C, and indeed, the spectrum shown in Fig. C.1c for $C = 2$ is identical to the original one with $C = 0$. Only the occupied and unoccupied states have been shuffled.

The precise way in which this shuffling is done cannot be found using only the instantaneous spectrum. However, in the adiabatic approximation the Chern–Simons number has an implicit time dependence, and this gives a relation between the (un)occupied states for different values of C, by continuity. For instance, states that seem to disappear from the spectrum at $(p = \pm\pi, E)$ return at $(p = \mp\pi, E)$, because of the periodicity of the lattice. A calculation of Q_5 shows that the contributions from the + and the − branch no longer cancel, and we find

$$Q_5(C) - Q_5(0) \approx C - 0,$$

which is of course the anomaly equation. Here it is important that states that are close to the continuum, i.e. with $|E_p| \ll 1$, do have an axial charge of approximately ± 1. This is not the case for states deep in the Dirac sea (see Eq. (C.1)).

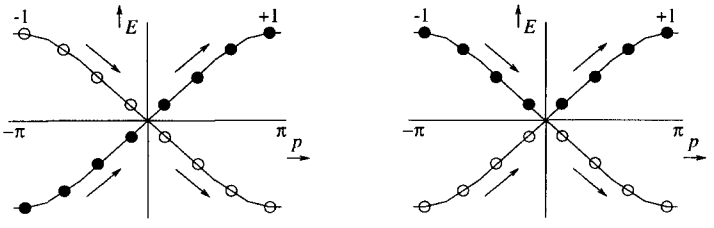

Fig. C.2. As in Fig. C.1, for (a) $C = N$, with maximal Q_5, (b) $C = 2N$, the filled Dirac sky.

We continue and look at larger Chern–Simons numbers. Since we only have a finite number of states, at some point all the occupied states have moved to the + branch. This is shown in Fig. C.2a. In our model this happens when $C = N$. This particular distribution of occupied states has the largest axial charge that is possible in the lattice model, and it is given by

$$\frac{Q_{5\max}}{N} = \frac{1}{N}\sum_p \frac{|s_p|}{E_p} \overset{N\to\infty}{\longrightarrow} 2\int_0^\pi \frac{dp}{2\pi}\frac{s_p}{E_p} = \frac{2}{\pi}, \tag{C.4}$$

where the last expression is valid in the limit $N \to \infty$. When we continue to even larger Chern–Simons numbers, all the occupied states end up in the Dirac sky, and the Dirac sea has completely dried up, as shown in Fig. C.2b. The axial charge is zero again.

It is clear that for these large values of the Chern–Simons number, lattice artefacts are substantial.

References

[1] F. Cooper and E. Mottola, Phys. Rev. D 36 (1987) 3114.
[2] F. Cooper, S. Habib, Y. Kluger, E. Mottola, J.P. Paz and P.R. Anderson, Phys. Rev. D 50 (1994) 2848.
[3] D. Boyanovsky, H.J. de Vega and R. Holman, Erice Lectures on Inflationary Reheating, at International School of Astrophysics, D. Chalonge: 5th Course: Current Topics in Astrofundamental Physics, Erice, Italy, 7–15 Sep. 1996, and references therein.
[4] Y. Kluger, J.M. Eisenberg, B. Svetitsky, F. Cooper and E. Mottola, Phys. Rev. Lett. 67 (1991) 2427; Phys. Rev. D 45 (1992) 4659.
[5] D. Boyanovsky, D. Cormier, H.J. de Vega, R. Holman and S.P. Kumar, Phys. Rev. D 57 (1998) 2166; D. Boyanovsky, D. Cormier, H.J. de Vega, R. Holman, A. Singh and M. Srednicki, Phys. Rev. D 56 (1997) 1939;
D. Boyanovsky, H.J. de Vega, R. Holman and J.F.J. Salgado, Phys. Rev. D 54 (1996) 7570.
[6] J. Baacke, K. Heitmann and C. Pätzold, Phys. Rev. D 57 (1998) 6406; D 56 (1997) 6556; D 55 (1997) 7815.
[7] D. Boyanovsky, M. D'Attanasio, H.J. de Vega, R. Holman and D.-S. Lee, Phys. Rev. D 52 (1995) 6805; J. Baacke, K. Heitmann and C. Pätzold, Phys. Rev. D 58 (1998) 125013;
P.B. Greene and L. Kofman, Phys. Lett. B 448 (1999) 6.
[8] F. Cooper, Y. Kluger, E. Mottola and J.P. Paz, Phys. Rev. D 51 (1995) 2377;
D. Boyanovsky, H.J. de Vega, R. Holman and S. Prem Kumar, Phys. Rev. D 56 (1997) 5233; D 56 (1997) 3929.
[9] F. Cooper, S. Habib, Y. Kluger and E. Mottola, Phys. Rev. D 55 (1997) 6471.

[10] V.A. Rubakov and M.E. Shaposhnikov, Usp. Fiz. Nauk 166 (1996) 493;
M. Trodden, hep-ph/9803479.
[11] D.Yu. Grigoriev, V.A. Rubakov and M.E. Shaposhnikov, Nucl. Phys. B 326 (1989) 737;
A.I. Bochkarev and Ph. de Forcrand, Phys. Rev. D 44 (1991) 519;
Ph. de Forcrand, A. Krasnitz and R. Potting, Phys. Rev. D 50 (1994) 6054.
[12] W.H. Tang and J. Smit, Nucl. Phys. B 540 (1999) 437.
[13] S.A. Ramsey, B.L. Hu and A.M. Stylianopoulos, Phys. Rev. D 57 (1998) 6003;
D. Boyanovsky, H.J. de Vega, D.S. Lee, Y.J. Ng and S.Y. Wang, Phys. Rev. D 59 (1999) 105001.
[14] K.G. Wilson, *in* New Phenomena in Subnuclear Physics, ed. A. Zichichi, Erice 1975 (Plenum, New York, 1977).
[15] L.H. Karsten and J. Smit, Nucl. Phys. B 183 (1981) 103.
[16] I. Montvay and G. Münster, Quantum Fields on a Lattice (Cambridge Univ. Press, Cambridge, 1994);
H.J. Rothe, Lattice Gauge Theories, An Introduction (World Scientific, Singapore, 1992).
[17] W. Bock, J.E. Hetrick and J. Smit, Nucl. Phys. B 437 (1995) 585.
[18] A.I. Bochkarev and M.E. Shaposhnikov, Mod. Phys. Lett. A 12 (1987) 991.
[19] L. Susskind, Phys. Rev. D 16 (1977) 3031;
M.F.L. Golterman and J. Smit, Nucl. Phys. B 245 (1984) 61.
[20] G. Aarts and J. Smit, in preparation.
[21] J. Smit, Nucl. Phys. B (Proc. Suppl.) 20 (1991) 542.
[22] J. Ambjørn, K. Farakos, S. Hands, G. Koutsoumbas and G. Thorleifsson, Nucl. Phys. B 425 (1994) 39.
[23] J. Ambjørn, J. Greensite and C. Peterson, Nucl. Phys. B 221 (1983) 381.
[24] K. Kajantie, M. Karjalainen, M. Laine, J. Peisa and A. Rajantie, Phys. Lett. B 428 (1998) 334.
[25] D. Bödeker, L. McLerran and A. Smilga, Phys. Rev. D 52 (1995) 4675.
[26] G. Aarts and J. Smit, Phys. Lett. B 393 (1997) 395; Nucl. Phys. B 511 (1998) 451.
[27] A. Messiah, Quantum Mechanics, Ch. XVII (North-Holland, Amsterdam, 1962).